An Investigation of GRID and Spatially Fractionated Radiation Therapy: Dosimetry and Preclinical Trial

by

Timothy Johnson

Department of Medical Physics
Duke University

Date:_______________________

Approved:

____

Mark Oldham, Advisor

____

Yvonne Mowery

____

Greg Palmer

Thesis submitted in partial fulfillment of
the requirements for the degree of Master of Science in the Graduate Program of
Medical Physics in the Graduate School
of Duke University

2021

<u>ABSTRACT</u>

An Investigation of GRID and Spatially Fractionated Radiation Therapy: Dosimetry and Preclinical Trial

by

Timothy Johnson

Department of Medical Physics
Duke University

Date:_______________________

Approved:

____
Mark Oldham, Advisor

____
Yvonne Mowery

____
Greg Palmer

An abstract of a thesis submitted in partial
fulfillment of the requirements for the degree
of Master of Science in the Graduate Program in
Medical Physics in the Graduate School of
Duke University

2021

Abstract

Purpose: To develop and implement novel methods of extreme spatially fractionated radiation therapy (including GRID therapy) and subsequent evaluation in pre-clinical mice trials investigating the potential of novel radiation treatments with potential for promoting anti-cancer immunogenic response.

Methods: Spatially fractionated GRIDs were designed and precision-milled from 3mm thick lead sheets compatible with mounting on a 225 kVp small animal irradiator (X-Rad). Three pencil-beam GRIDs created arrays of 1mm diameter beams, and three "bar" GRIDs created 1x20mm rectangular fields. GRIDs projected 20x20mm fields at isocenter and beamlets were spaced at 1, 1.25, and 1.5mm, respectively. Output factors, peak-to-valley ratios, and dose distributions were determined with Gafchromic film. The bar GRID with 1mm beamlet spacing (50% area treated) was selected for the pre-clinical trial. Soft-tissue sarcoma (p53/MCA) was transplanted into C57BL/6 mice's flanks. Four treatment arms were compared: unirradiated control (n=18), conventional irradiation of the entire tumor (n=16), GRID therapy (n=17), and hemi-irradiation (n=17) where one-half of the beam was blocked. All irradiated mice received a single fraction of 15 Gy to irradiated regions. To date, this is the first study to compare GRID treatment against conventional RT at the same dose.

Results: Very high peak-to-valley ratios were achieved (bar GRIDs: 11.9±0.9, 13.6±0.4, 13.8±0.5; pencil-beam GRIDs: 18.7±0.6, 26.3±1.5, 31.0±3.3). Pencil-beam GRIDs spared twice the number of intra-tumor immune cells as bar GRIDs but left more of the tumor untreated (2-3% vs 14-17% area receiving 95% prescription, respectively). Penumbra was halved when GRIDs were 50% closer to treatment isocenter. The GRID selected for mouse trials was theoretically capable of sparing approximately 15% of intra-tumor CD8+ and CD4+ T cells (this value assumes a D_{50} of 1.5 Gy for the lymphocytes, and the amount of lymphocytes in tumors was not measured in the trials). Preliminary results indicate mean times to tumor quintupling were: 12, 13, 14, and 20 days for unirradiated, GRID, hemi-irradiated, and conventional treatment groups, respectively. To date, all tumors have quintupled except for nine in the full irradiation group.

Conclusions: Peak-to-valley ratios with kV grids were substantially superior to MV grids, which historically achieve ratios between 2.5 and 6.5. In data collected to date, GRID and hemi-irradiation did not significantly delay tumor growth as compared to an unirradiated control (P = 0.122 and P = 0.2437, respectively, P-values from logrank analysis). Differences between GRID and hemi-irradiation were not statistically significant (P = 0.5257). To date, the conventional RT group has performed significantly better than all other groups (P<0.001). These results do not corroborate the success of hemi-irradiation in Markovsky et al. 2019. GRID treatments may be more effective if a substantially higher dose and/or multiple fractions were employed.

Contents

List of Tables

List of Figures

Acknowledgements

This project had many moving parts, and it could not have happened without help from these people. Thank you to Jelinek and Richard Nappi at the Physics Instrument Shop for machining the GRIDs and answering all my questions about materials and designs. Thank you to Nerissa Williams for performing irradiations and giving feedback on our treatment techniques. Thank you to Collin Kent and Alex Bassil for their work measuring and caring for mice. Thank you to Dr. Greg Palmer for vital insights on evaluating GRIDs. Thank you to Dr. Yvonne Mowery for your commitment to the project. Thank you to the previous students—Paul Yoon, Devin Miles, Deqi Chen, and Jacob Kodra—for laying the foundation of this experiment. Thank you to my lab mates Russel Holden and Scott Hoopingarner for talking through the project and listening to a dozen journal club presentations. Thank you to Simon Brundage for your instant interest in the project. Lastly, thank you to my advisor, Dr. Mark Oldham, for starting this investigation and teaching me to grow as a physicist.

1. Introduction

1.1 GRID Therapy Definition and Background

GRID therapy is a type of radiation therapy that treats tumors with an array of small beams. The small beams are typically created by placing a physical block in the path of a single, large beam. The block, called a "GRID," is a radiation-blocking material with an array of openings allow sections of the large beam through. Example materials for GRIDs are lead, bronze, and Cerrobend. GRID is a subtype of Spatially Fractionated Radiation Therapy (SFRT), which encompasses treatments that irradiate only part of a tumor instead of its entire volume.

Healthcare providers first used GRID therapy with megavoltage beams in 1990 (Mohiuddin et al. 1990). The technique was used as a palliative treatment for bulky tumors that were inoperable or had resisted conventional RT techniques. A 15 x 15 cm array of pencil beams allowed single fractions of 10-15 Gy to be delivered with few normal tissue complications. The GRID treated 50% of the tumor (also known as a 50:50 "open-to-closed ratio"), which became a standard for future treatments (Yan et al. 2020). GRID was used as a boost to conventional RT, and 20 of 22 radioresistant tumors showed palliative responses. In the following years, GRID experiments continued in both curative and palliative settings with similar results (Yan et al. 2019, Griffin et al. 2020). These treatments used doses between 10 and 25 Gy, but rates of normal tissue complications were low: one study of 53 patients who received 15 Gy showed only 4% of subjects develop grade 3 or worse toxicity (Edwards et al. 2015), and a study of 71 patients receiving 10-20 Gy had no toxicity, though there was a single carotid blowout (Mohiuddin 1999). GRID has been applied to many tumor locations including the lungs, GI, and breasts, but most trials have targeted head and neck cancers (Yan et al. 2019). In these groups, overall response rates have varied from 50-90%.

There have been some attempts at creating GRID patterns using multi-leaf collimators (MLCs) to create arrays of beams instead of physical blocks. The MLC-GRID treatments (n=40) were compared with Cerrobend-GRID treatments (39), and both treatments had similar rates of tumor response and normal-tissue complications (Neuner et al. 2012). However, another study showed that MLC-GRID treatments require a six-fold increase in treatment time, and the array of beams is blurred due to MLC leakage and high MU (Buckey et al 2010).

1.2 Biological Response to GRID Therapy

Despite the positive clinical outcomes of GRID treatments, many of the biological underpinnings of spatial fractionation are not well understood (aside from palliative debulking). There are, however, promising studies regarding beam size, bystander effects, abscopal effects, and immunostimulation.

1.2.1 Normal-Tissue-Sparing of Small Beams

There is growing evidence that small beams cause fewer complications in healthy tissue than large beams (Griffin et al. 2020). A study of beams between 6 mm and 0.5

mm showed that decreasing beam diameter also reduced skin complications in mouse ears, especially when beams were less than 2 mm in diameter (Sammer et al. 2019). Despite the small size of the beams, numerous studies have shown that beams with diameters of 50 μm and smaller can damage tumors (Bouchet et al. 2013, 2015, Serduc et al. 2009).

1.2.2 Bystander and Abscopal Effects

Bystander effects are effects observed in unirradiated cells near irradiated cells. The irradiated cells emit cytokines that may cause effects including apoptosis and DNA damage. GRID therapy has been shown to cause *in vitro* bystander effects in murine cancer models. Cancer cells located between two GRID-produced pencil beams received less than 1 Gy, but their survival rates were significantly lower than cells that received 1 Gy from a planar beam (Asur et al. 2012). These effects have been noted in other spatial fractionation techniques, notably in bulky, hypoxic tumors (Tubin et al. 2019).

Abscopal effects are tumor-controlling effects in locations distant from irradiated cells, such as untreated metastases. One study noted that patients who received GRID treatments of head and neck squamous cell carcinoma exhibited lower rates of distant metastasis than historical controls, suggesting that abscopal effects may have been induced (Edwards et al. 2015). Two studies in mice implanted with Lewis Lung Carcinoma indicated that partial-volume irradiations cause more significant abscopal effects than conventional RT (Kanagavelu et al. 2014, Markovsky et al. 2019).

1.2.3 Immunostimulation

Tumor cells have mechanisms to avoid detection by the immune system. A notable mechanism is that cancer cells conceal antigens that denote them as tumors, which prevents immune cells from signaling a response. However, some studies indicate that ionizing radiation can overcome tumor cloaking mechanisms (Kaur and Asea 2012, Chakraborty et al. 2004). Following irradiation, tumor antigens are released and may be detected by immune cells, which then summon tumor-killing CD8+ T cells (Sologuren et al. 2014).

Spatial fraction may be able to stimulate immune responses (Griffin et al. 2020). First, abscopal effects have been attributed to immune responses (Demaria et al. 2004). Second, SFRT's normal-tissue-sparing effects may help preserve the immune system during treatment. While conventional treatments irradiate all the immune cells throughout and near tumors, GRID therapy can minimize dose to immune cells in the target tissues. The valleys of GRID dose distributions would spare lymphocytes and possibly allow them to rapidly identify tumor antigens following treatment, which would lead to prompt activation of the immune system's anti-tumor cells. Lymphocytes are conventionally taken as radiosensitive because a dose of 1.5 Gy can kill approximately 50% of circulating CD8+ T cells (Nakamura et al. 1990). However, recent studies show that resident T cells that have been activated to fight tumors may be much more radioresistant, even up to 20 Gy (Hu et al. 2018). GRID therapy may be key in sparing T cells that have not yet been activated.

Two SFRT studies in murine cancers show heightened CD8+ T cell responses following partial-volume irradiation (Kanagevalu et al. 2014, Markovsky et al. 2019). Most notably, the Markovsky study showed that hemi-irradiation (irradiation of only 50% of an area) of a murine tumor could produce abscopal effects, cause heightened CD8+ T-cell infiltration in the tumor, and achieve tumor control and cure rates comparable to conventional RT at the same doses. Furthermore, hemi-irradiation was ineffective when the immune system was inhibited. These effects were observed in 67NR breast cancer in BALB/C mice and in Lewis lung cancer in C57BL/6 mice. The Markovsky study had tremendous implications for immunostimulation and spatial fractionation because it supported radical treatment methods.

1.3 Scope

Several aspects of GRID therapy and spatial fractionation remain to be investigated. Despite many trials in humans, GRID therapy has almost always been studied as a boost to conventional treatment schemes instead of as an independent treatment method. Also, no studies have investigated the ideal pattern of spatial fractionation. I.e., would an array of small beams that irradiate half a tumor lead to better tumor control than a single beam that also covers 50% of a tumor?

This thesis had several goals:

1. To design and manufacture GRIDs for a small animal irradiator and characterize their dosimetric properties. GRIDs would ideally be able to spare immune cells in the valleys of the dose distribution while maintaining high dose peaks to damage tumor cells.
2. To investigate the feasibility of various GRID treatments for small animals with an X-Rad 225Cx system, including accuracy of the setup, effects of motion, and treatment time.
3. To evaluate tumor growth delay of mice receiving conventional, GRID, and partial-volume radiation therapy treatments. The partial volume trial aims to reproduce Markovsky et al. 2019, which had exceptional rates of tumor control despite irradiating only 50% of tumor volumes.

2. Methods

2.1 GRID Design

GRIDs were designed in Fusion 360, a 3D modeling software available to Duke students. The physical GRIDs were machined by Duke's Physics Instrument Shop.

2.1.1 Peak-to-valley ratio and lymphocyte sparing

A useful metric for characterizing a GRID is its peak-to-valley ratio, which is defined as the peak dose of the beamlets divided by the dose delivered under the blocked sections of the GRIDs (Reiff et al. 1995, Buckey et al. 2010, Bazyar et al. 2017). A high peak:valley is preferable because it indicates that high doses can be delivered to the tumor while sparing normal tissue. The goal of these GRIDs was to spare lymphocytes, which can lose 90% of their population after receiving 3.1 Gy (Nakamura et al. 1990). A maximum valley dose of 1.5 Gy was chosen as a goal to spare at least 50% of CD8+ T cells in valleys during *in vivo* trials.

2.1.2 Material and thickness

GRIDs were designed for use on the X-RAD 225Cx small animal irradiator (Precision X-Ray, N. Banfield, CT) with its standard 225 kVp beam energy. Thin GRID designs were preferable for ease of attaching to the irradiator. Additionally, a thick GRID would have to be machined to match the divergence of the beam. Lead was chosen as the GRID material for its high density and mass-attenuation coefficient. Attenuation of the beam was calculated with the equation:

$$\frac{I}{I_0} = e^{-\mu t} \qquad \textit{(Eq. 1)}$$

Where μ is the attenuation coefficient, t is the thickness of the material, I_0 is the initial intensity of the beam, and I is the final intensity. Values of μ were derived from the mass-attenuation coefficients provided by NIST. For a worst-case, pure 225 kV beam, three millimeters of lead would reduce the beam to 6.58% intensity. However, a 225 kVp beam has an average energy of approximately 75 kV, which three millimeters of lead would reduce to less than 0.005% intensity. Three millimeters was chosen as an optimal thickness for the GRIDs.

2.1.3 Beamlet pattern

A key aspect of GRID design that has been largely unexplored is the impact of beam arrangement on dosimetry and treatment outcomes. Some factors that can be adjusted are the shape of the beams, the spacing between beamlets, and the percentage of area treated (the amount of beam unblocked by the GRID). Because these parameters have rarely been evaluated within one experiment, several GRIDs with different designs were created.

2.1.3.1 Pencil-beam GRIDs

All GRIDs employed in human trials have created pencil beams. Figure A shows several examples of these GRIDs, which arrange their beams in either square or hexagonal arrays. Figure 1 shows several examples of GRIDs with pencil beam arrangements.

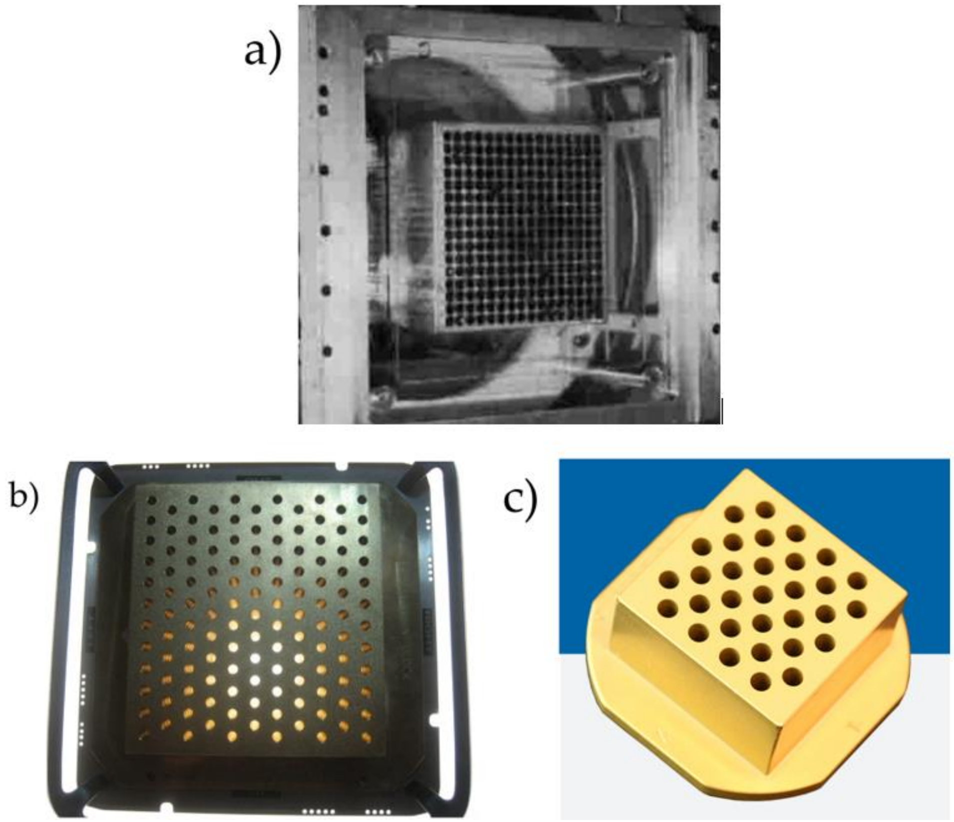

Figure 1: Example pencil-beam GRIDs. a) One of the first GRIDs developed for MV irradiators (Mohiuddin et al. 1996). b) A GRID mounted on a block tray (Buckey et al. 2010). c) A commercially available GRID (.decimal.com).

Square and hexagonal arrays have an important difference, which is shown in Figure 2. In a hexagonal arrangement, each beamlet is equidistant from all its neighbors. The valley dose between each pair of holes will ideally be the same across all pairs. However, a square array has diagonal neighbors, which are farther apart than axial neighbors. The valley dose between diagonal neighbors will not be equal to the dose between vertically or horizontally adjacent neighbors. The discrepancy in valley dose is problematic when characterizing GRIDs. While a hexagonal GRID only has one peak-to-valley ratio because all the holes are equidistant, a square GRID has an additional peak-to-valley ratio along its diagonal plane. In other words, square GRIDs create less consistent dose distributions than hexagonal GRIDs. For this reason, hexagonal designs were preferred over square designs.

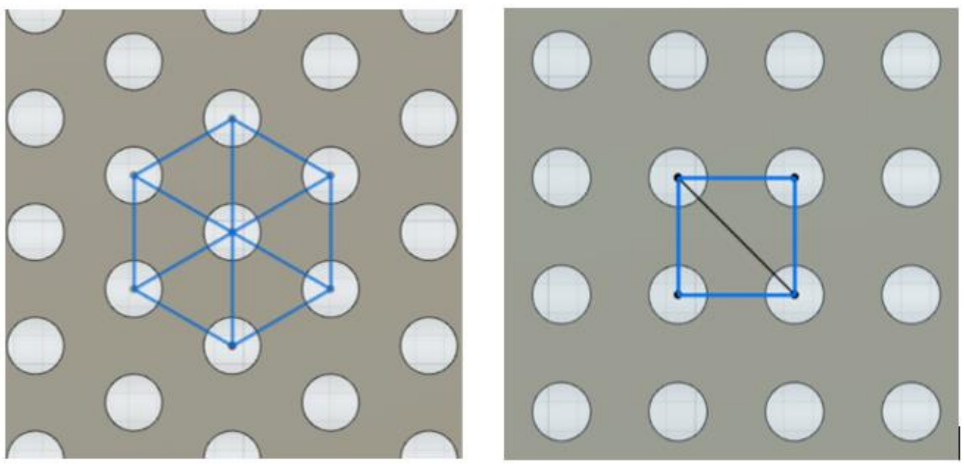

Figure 2: Center-to-center distances between holes in hexagonal GRIDs (left) and square GRIDs (right). Blue lines are equidistant.

2.1.3.2 Bar GRIDs

Bar GRIDs are a new type of arrangement that recently garnered attention for mice trials (Bazyar et al. 2017, Treibel et al. 2020). Instead of pencil beams, these GRIDs produce long rectangular beams that create contiguous treatment zones. An example bar GRID design is shown in Figure 3. The pictured GRID was used to deliver a peak dose of 150 Gy to mice, which controlled B16-F10 melanoma tumors with minor normal tissue complications. The radiobiological effects of bar GRIDs as compared to pencil-beam GRIDs are currently unknown.

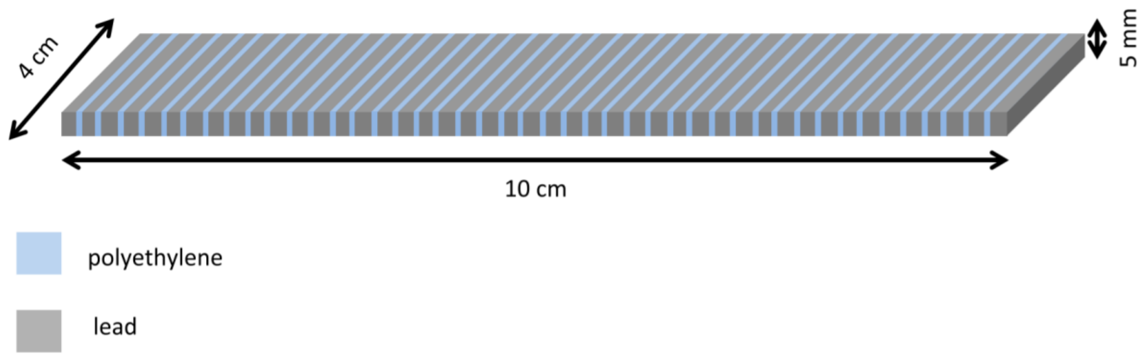

Figure 3: A "minibeam collimator" with alternating layers of lead and plastic to create blocked and unblocked areas (Bazyar et al. 2017). Lead layers are 0.70 mm thick and plastic layers are 0.30 mm.

2.1.3.3 Percent area treated and beamlet spacing

A key tradeoff in GRID design is the target coverage versus the amount of normal tissue sparing. A GRID with shorter spacing between beams covers more of the target whereas a GRID with larger spacing increases the volume of spared normal tissue. Large spacing also separates the beams enough to maximize the peak-to-valley ratio. Although larger spacing should spare more lymphocytes to aid in the immune response, the radiobiological impacts of beam spacing have not been tested. Studies in humans have only used GRIDs that block 50% of the field (Mohiuddin et al. 1990, 1996, 1999, Griffin et al. 2020), though a 2017 mouse trial used a GRID that was 33% open (Bazyar et al. 2017).

For the purposes of this experiment, bar GRIDs had a key advantage over pencil-beam GRIDs. Bar GRIDs can achieve high target coverage with large spacing, but pencil-beam GRIDs require many holes with short spacing to treat 50% of the tumor. Lead is a soft metal, so the pencil-beam designs were especially susceptible to deforming during machining processes. Three beam spacings were chosen for evaluation: 1 mm, 1.25 mm, and 1.5 mm of lead between beams.

Six GRIDs were developed as candidates for mice trials: three bar GRIDs and three hexagonal pencil-beam GRIDs. Each set had a GRID with 1, 1.25, and 1.5 mm spacing. The pencil beams and bars had diameters of 1 mm, and the GRIDs were designed to convert large fields into arrays of beamlets with fields sizes of approximately 20x20 mm^2. These GRIDs are shown attached to block trays in Figure 4.

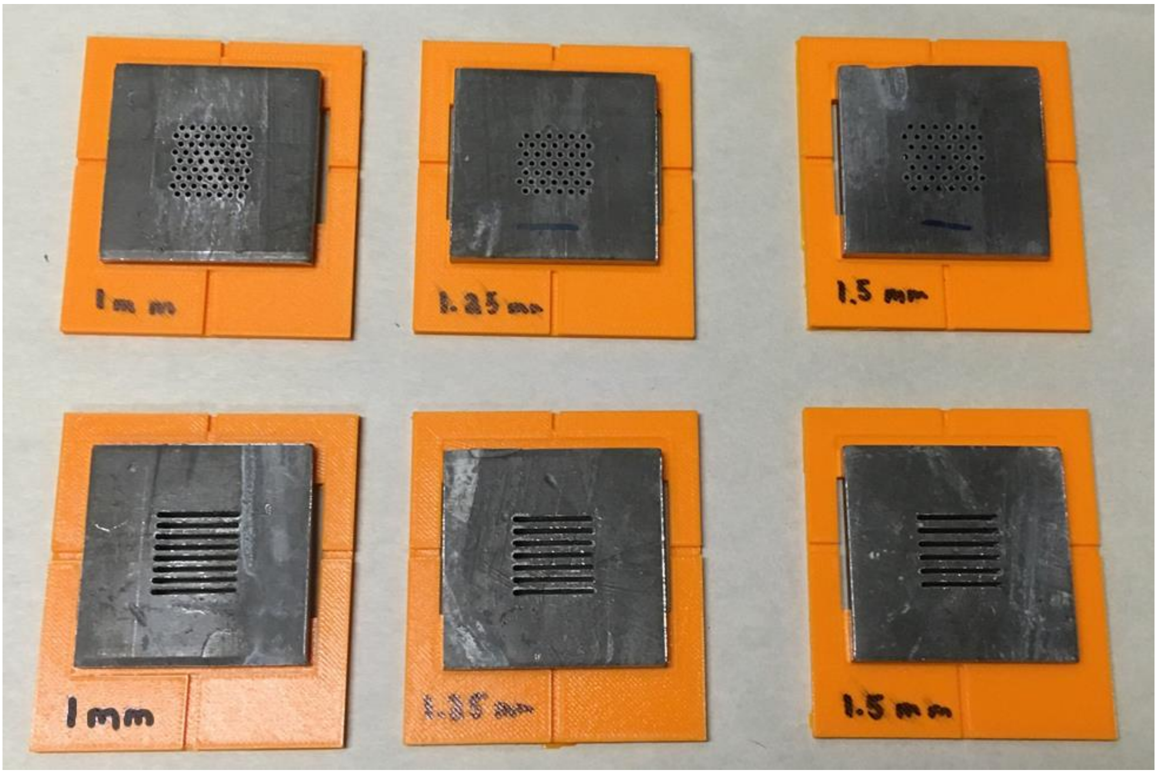

Figure 4: GRIDs developed for use on the small animal irradiator. The top GRIDs are pencil-beam GRIDs with a hexagonal arrangement of beams, and the bottom GRIDs are bar designs. The GRIDs are attached to 3D-printed block trays for mounting on the XRAD-225Cx.

2.2 GRID Dosimetry

2.2.1 Gafchromic film and scanning

EBT3 Gafchromic film was used for all dosimetry measurements. Before and after irradiation, films were scanned on a 12000XL Epson scanner using the Epson Scan 2 program. The scanner was allowed 1 hour of warmup time before scanning to mitigate inhomogeneous measurements. After irradiation, the films were allowed 24 hours to self-develop before the post-scan. Films were kept in dark envelopes when not in use.

The transmission through the films were measured in ImageJ by drawing regions of interest (ROIs). Only the red channel of the images was used for analysis of the EBT3 films. The change in optical density was found with the following equation:

$$\Delta OD = \log_{10}\left(\frac{I_{Before}}{I_{After}}\right) \qquad \textit{(Eq. 2)}$$

I_{Before} is the intensity of light transmitted through the film prior to irradiation, and I_{After} is the intensity of transmitted light after irradiation. Film was given 24 hours to develop after irradiation.

2.2.2 Basic setup and film calibration

All irradiations were performed with the XRAD 225Cx using a 225 kVp beam and a current of 13 mAs. The 40 mm x 40 mm cone was used for these initial measurements. Films were placed on top of a solid water block to emulate backscatter conditions from tissue, and films were placed at isocenter. A calibration curve was generated for this batch of EBT3 film by irradiating films with 0, 0.5, 1, 2, 3, 4, 5, and 6 Gy. ROIs were drawn in ImageJ in the irradiated areas, and the mean pixel value of each found for pre-scans and post-scans. These values were converted to change in optical density using Equation 2. These data points were fit to a third-order polynomial as in the XRAD 225Cx commissioning paper (Newton et al. 2012). The calibration curve is shown in Figure 5, and its equation was used to find the relationship between change in optical density and dose for this batch of film. This equation was used to calculate dose delivered to other films.

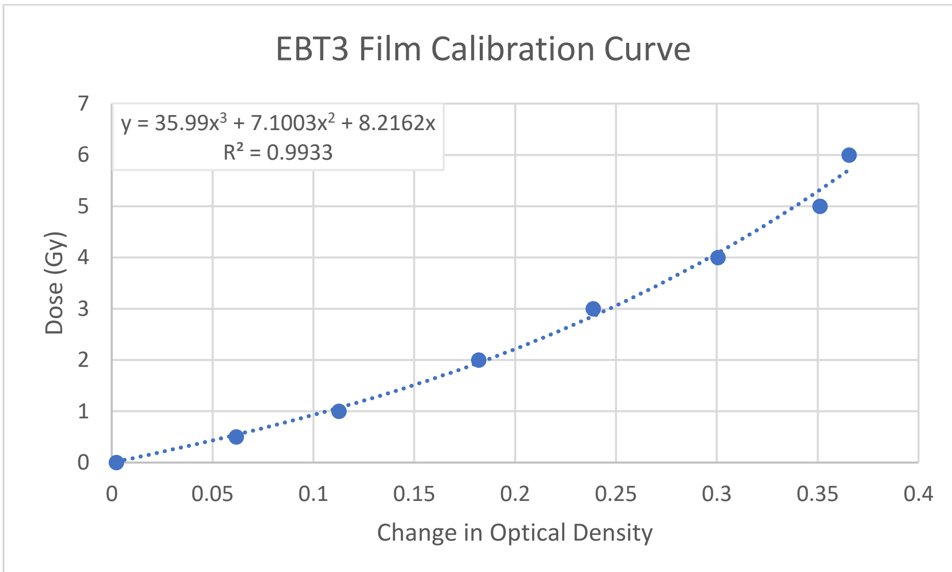

Figure 5: Calibration curve for EBT3 Gafchromic film. Curve was generated November 10th, 2020 for a newly purchased batch of film.

2.2.3 Output factors and peak:valley measurements

To determine the output factors of the GRIDs, they were inserted into a 3D-printed block tray devised a by Deqi Chen, a previous student in Oldham lab. As in the calibration curve measurements, films were placed on a solid water block, the films were at isocenter, and the 40x40 mm^2 cone was used. The beam was on for 108 seconds, which is the time taken to deliver 6 Gy with the unblocked 40x40 mm^2 cone. The output factor of each GRID was found with the following equation:

$$\text{Output} = \frac{Avg\ Peak\ Dose}{6\ Gy} \quad \textit{(Eq. 3)}$$

Peak-to-valley ratios are measured as the maximum dose of a peak divided by the minimum value of its adjacent valleys (Mohiuddin et al. 1996, Buckey et al. 2010). In ImageJ, line profiles were drawn through the central axis of each GRID, as shown in Figure 6. Each line profile's data was converted into quantitative list. Dose was found for each point by applying Equation 2 to each value in the list. A 3-pixel-radius median filter was applied to the images before analysis. The median filter reduced noise but preserved the steep gradients of the peaks and valleys.

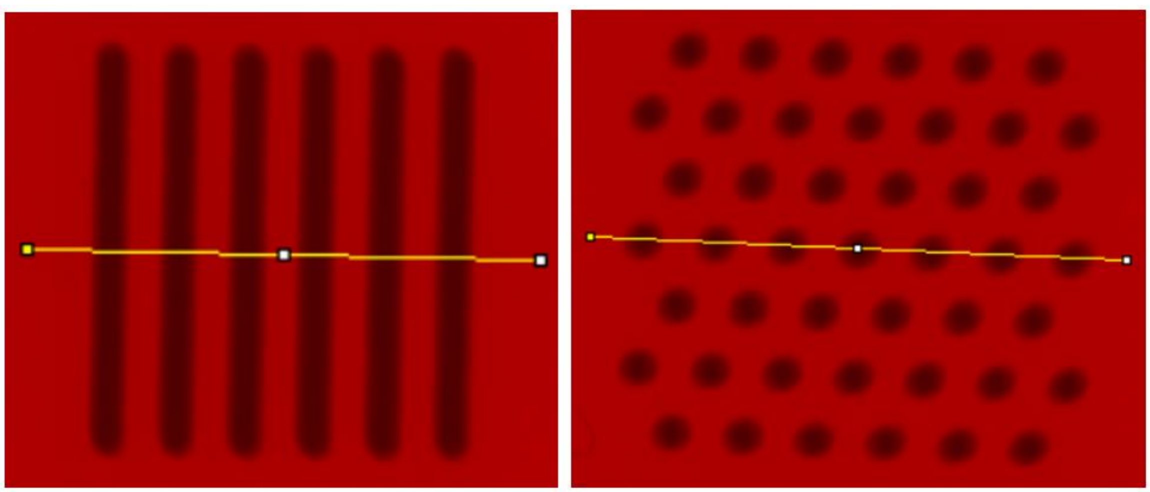

Figure 6: Example line profiles through the bar GRID (right) and pencil-beam GRID (left) with 1.5 mm spacing between beamlets. Results shown in Figure 15.

2.2.4 Dose maps

Scans of films were converted into maps of absolute dose using the calibration curve and an in-house MATLAB script. These dose maps were converted to relative dose maps by dividing each pixel's absolute dose by the average dose of each GRID's peaks. These dose maps are shown in Figure 7. Each field is approximately 20x20 mm^2.

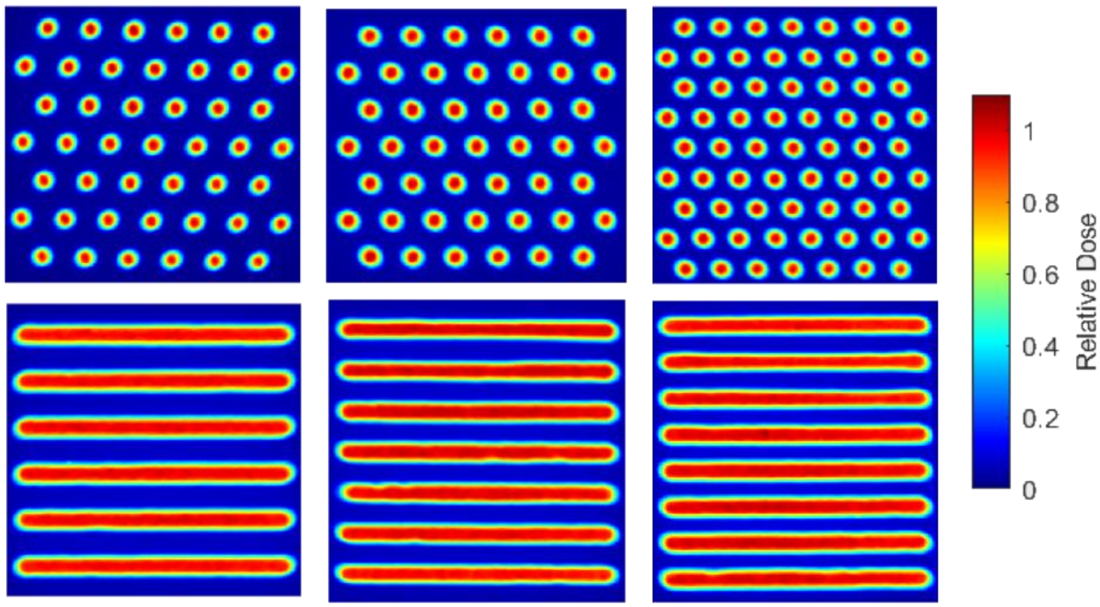

Figure 7: Dose maps of GRIDs. Top: Pencil-beam GRIDs. Bottom: Bar GRIDs. Left-to-Right: 1.5, 1.25, 1 mm beamlet spacing.

2.2.4.1 Treatment area above and below dose thresholds

Although peak-to-valley ratios are a conventional measurement for GRIDs, they do not define the amount of spared intra-tumoral lymphocytes. The goal of these GRIDs was to reduce valley dose to less than 1.5 Gy, which is the D_{50} for CD8+ and CD4+ T cells (Nakamura et al. 1990). Given a 15 Gy treatment, the valley dose should be 10% or less than the treatment dose. To find the amount of tissue in the treatment zone receiving less than 1.5 Gy, the dose maps were binned by dose values. The number of pixels receiving less than 10% prescription dose was compared to the total number of pixels in the field (approximately 20 x 20 mm for each GRID), which gave a percentage of tissue spared by each GRID. This process was repeated for 3.1 Gy, the D_{90} of CD4+ and CD8+ T cells. The percent areas receiving above 15 Gy (the prescription dose) and above 95% prescription dose were also calculated.

2.2.4.2 Dose volume histograms

A dose volume histogram (DVH) is a chart that shows the percentage of tissue that is receiving dose. DVHs are commonly used in treatment planning software as a way to represent dose to organs and tumors. A DVH for each GRID was generated in MATLAB from the dose maps shown in Figure 7. These DVHs represent the dose distributions at isocenter.

2.2.4.3 Integral dose relative to open field

Integral dose is a measure of the total dose delivered during a treatment, and it is given by the equation (Slosarek et al. 2015):

$$Integral\ Dose\ =V_{tissue} * D_{average} \qquad \textit{(Eq.5)}$$

Each GRID's integral dose was compared to the integral dose delivered by an open field of the same size. In the above equation, the tissue volume (V_{tissue}) would be constant across GRID and open-beam trials, so relative integral dose of one field divided by another simplifies to:

$$Relative\ Integral\ Dose\ =\frac{(D_{average})_{GRID}}{(D_{average})_{Open}} \qquad \textit{(Eq.5)}$$

$(D_{Average})_{Open}$ was assumed to be 15 Gy, and $(D_{Average})_{GRID}$ was the mean dose calculated from each GRID's dose map. This metric of relative integral dose contextualizes how much dose each GRID delivers to tissue compared to a conventional treatment.

2.2.5 Evaluation of treatment setups and depth-dependence of dose distributions

2.2.5.1 Depth dependence

To characterize how GRID dose distributions may change with depth, a 3D-printed film holder (AKA "oven") was produced. Films could be inserted into slots in the oven at different heights. The oven was attached to a plastic bowl, and the bowl could be filled with water. In this way, a single irradiation could deliver dose to films at various depths. The water was filled up to the top slot in the oven, so the films were at depths of 0, 2.5, 5, 10, and 20 mm. All films except the surface film were submerged in water, and the deepest film had 10 mm of water beneath it. Figure 8 shows a prototype of the oven and the complete water setup.

The bar GRID with 1.5 mm beamlet spacing was used in this trial.

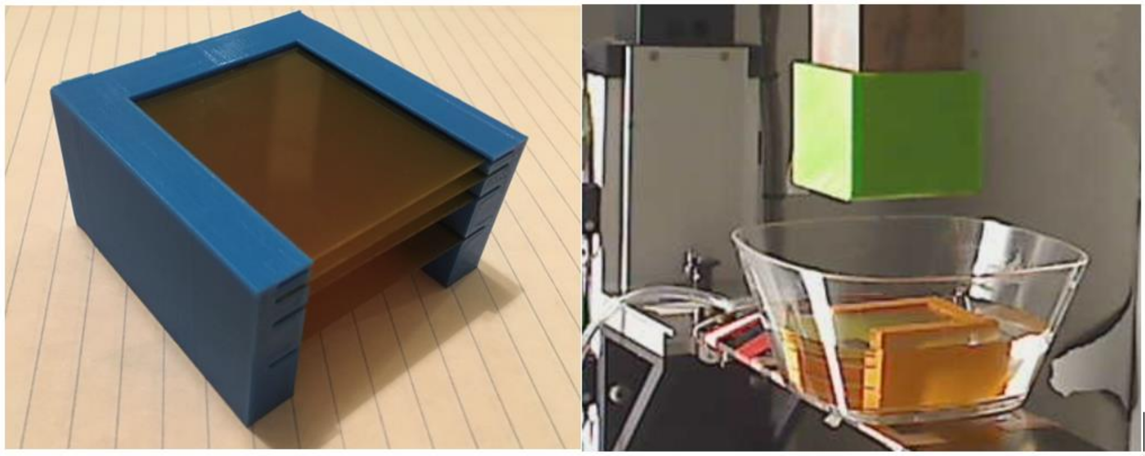

Figure 8: Left: prototype film holder. Right: water phantom with films in place on the treatment couch. Water was filled to the top film.

2.2.5.2 Block tray setup versus table setup

Although mounting GRIDs on the block tray provides a reproducible setup, the GRIDs were six centimeters from isocenter. It was theorized that placing the GRID closer to isocenter would reduce beam divergence, which would reduce the beams' penumbra, increase the width of valleys, and possibly increase the peak-to-valley ratio.

A 3D-printed table was developed to hold GRIDs over the treatment target. The table was 3 cm tall, and GRIDs were positioned over an opening in the table. Figure 9 shows the table design. Figure 10 shows both irradiation setups. The bar GRID with 1.5 mm bar spacing was used in this trial, and the treatment time was 108 seconds for both irradiations.

Line profiles were drawn ImageJ. The peak-to-valley ratios, valley widths (valleys were defined as regions between peaks that received 15% or less peak dose), and penumbral region widths (the regions receiving between 20% and 80% dose) were calculated in Excel.

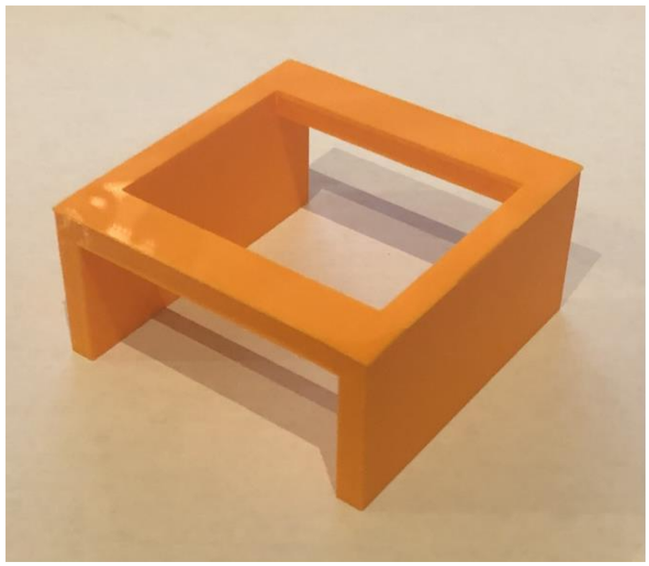

Figure 9: 3D-printed table for GRID mounting with extended SCD (24 cm extended to 27 cm). The table used in irradiations was 3 cm tall.

Figure 10: GRID setups tested with water phantom. Left: block tray setup. Right: Table setup.

2.2.6 Quantitative analysis of tumor motion

Motion is important in GRID therapy. Even sub-millimeter motions could blur a GRID's beams, which would distribute dose throughout the tumor instead of creating discrete peaks and valleys. To evaluate tumor motion's impact on GRID therapy, a 5 mm x 5 mm piece of film was attached to a tumor on a mouse's right flank. The leg with the tumor was taped to the treatment table as in a standard treatment. The mouse anesthetized but noticeably breathing. The pencil-beam GRID with 1 mm spacing was mounted on the block tray and used to treat the tumor for 108 seconds. The film received the central beam of the GRID. The treatment is shown in Figure 11. The trial was performed with four mice. One mouse had a tumor of standard treatment size (~70 mm^3), one mouse had a tumor larger than treatment size (~400 mm^3), and two mice had no tumors.

Beam width was defined as the full-width half max (FWHM) of the central beamlet's peak. Line profiles were drawn through the central beamlet at four different angles, as shown in Figure 12. The mean FWHM of the line profiles was found for the central beamlet of the GRID. The central beamlets from the motion trial and the earlier stationary trial were compared. In the stationary trial, the film was placed on a solid water block.

Figure 11: Treatment setup for the motion evaluation. The film is on the mouse's right flank and is not visible in this picture.

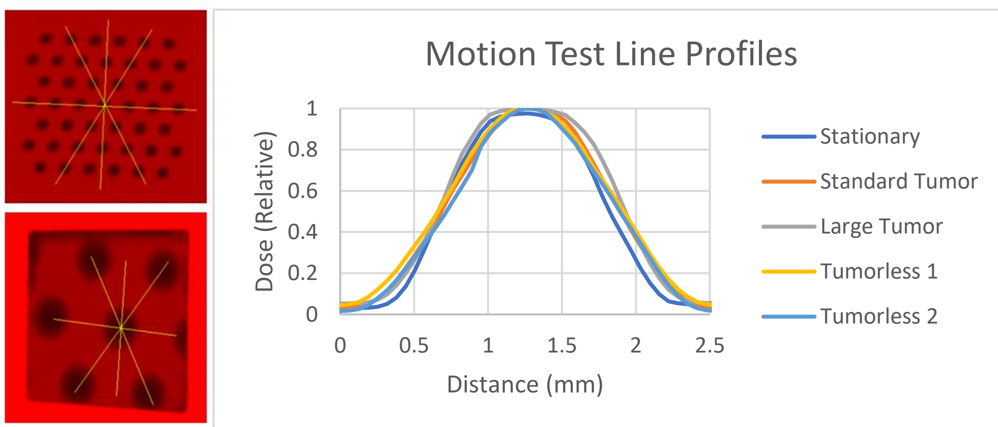

Figure 12: Sample line profiles for motion evaluation. The left images show profiles drawn in ImageJ, and the right image shows the vertical profile from each test. The pencil beam GRID with 1 mm spacing was used for evaluation.

2.3 Mice Trials

2.3.1 Mouse model

Forty C57BL/6 mice were purchased from Jackson Labs, and the p53/MCA transplant sarcoma model was used. Mice were injected with a p53 deactivator and a carcinogen, methylcholanthrene. Soft tissue sarcoma was transplanted into the right flank of the mice. Mice resided at Duke's Genome Science Research Building II, and they were entered into the experiment once their tumors were measured to be 65 cc or larger.

2.3.2 Treatment arms

Mice were divided into four treatment groups. All irradiated mice received 15 Gy in a single fraction using the 20 mm x 20 mm treatment cone. Mouse legs were taped to the treatment table for immobilization. The output of the beam was scaled for the cone using the output factor of 0.94 derived from the XRAD commissioning paper (Newton et al. 2012). The GRID treatment was scaled using the calculated output factor for the GRID.

1. Unirradiated control (18 mice)
2. Full irradiation (16 mice)
3. Bar GRID (17 mice)
4. Half block (17 mice)

The full irradiation group represented a conventional RT treatment, which served as a comparison for the spatially fractionated treatments. The bar GRID with 1 mm spacing was selected for the GRID trial, and the table setup was used. Figure 13 shows the table setup used for the experiment. The half block treatment arm replicated the Markovsky et al. experiment in which a contiguous half of the tumor was irradiated. To block half the treatment beam, a block was created by attaching a 3 mm thick sheet of lead to a block tray, which is shown is Figure 14.

Figure 13: Treatment setup for GRID and half block trials.

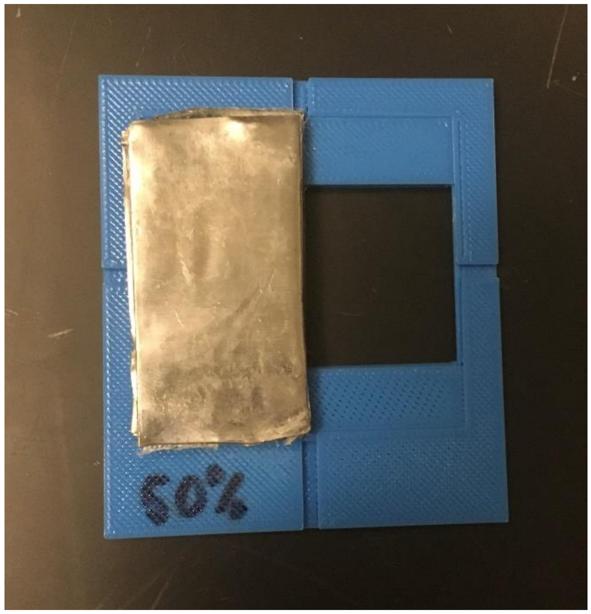

Figure 14: Lead sheet used for half block trials.

2.3.3 Tumor growth and survival

Mice tumors were measured every 2-4 days. Tumor size was recorded until tumors impacted the mice's quality of life, at which point the mice were sacrificed. Tumor quintupling was chosen as an endpoint for the experiment.

2.4 3D printing

Several objects were 3D-printed for this experiment. These objects include block trays, the film oven, and the table for the GRID and half block irradiations. These models were designed in Fusion 360 and printed at Duke's Innovation Co-Lab. All objects were printed using Ultimaker 3S printers with the fused filament fabrication method. PLA plastic was the only material used.

3. Results

3.1 GRID Characterization

3.1.1 Core GRID characteristics: precent area treated, output factors, and peak-to-valley ratios

GRID characteristics that are commonly used to describe GRIDs are shown in Table 1. “Percent area treated” refers to the proportion of the beam blocked by each GRID, and it is an adjustable parameter in the design process. GRIDs with smaller beamlet spacing allow more beam through, and bar GRIDs are significantly more open than pencil-beam GRIDs. Output factors are used to scale the dose output of the X-Rad 225Cx using the 40x40 mm^2 cone to the output when each GRID is being used.

Peak-to-valley ratios tend to increase as beamlet spacing increases, which is intuitive because the increasing material between beams reduces primary scatter. However, the bar GRIDs with beamlet spacings of 1.25 mm and 1.5 mm have very similar peak-to-valley ratios (13.6 ± 0.4 and 13.8 ± 0.5, respectively), which suggests that the bar GRIDs reached an upper limit on peak-to-valley improvements with spacing. In terms of comparing GRID patterns, peak-to-valley ratios of pencil-beam GRIDs are substantially higher than bar GRIDs because more of the beam is blocked by the GRID. Line profiles through the central axis of each GRID are shown in Figure 15.

Table 1: GRID characteristics.

GRID Pattern	Beamlet Spacing (mm)	% Area Treated	Output Factor	Peak:Valley
Bar	1	50%	0.69 ± 0.01	11.9 ± 0.9
	1.25	44%	0.68 ± 0.01	13.6 ± 0.4
	1.5	40%	0.71 ± 0.01	13.8 ± 0.5
Pencil Beam	1	23%	0.76 ± 0.02	18.7 ± 0.6
	1.25	19%	0.74 ± 0.01	26.3 ± 1.5
	1.5	16%	0.66 ± 0.02	31.0 ± 3.3

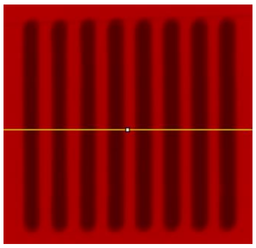

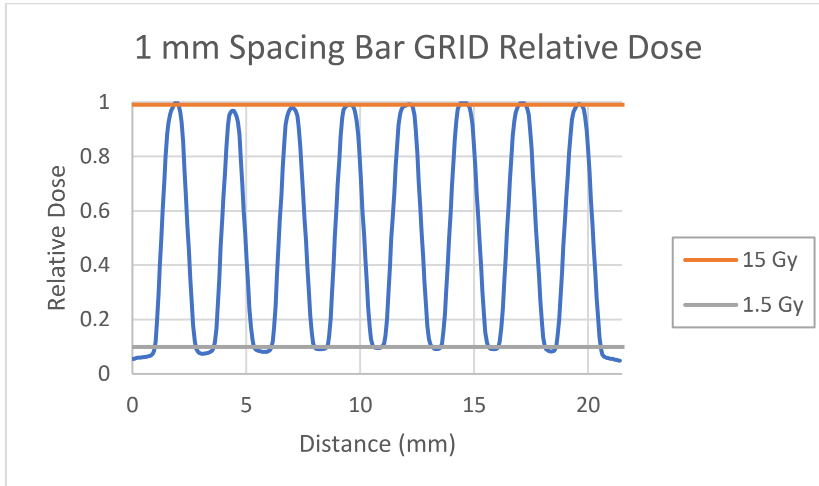
1 mm Spacing Bar GRID Relative Dose
Relative Dose
1
0.8
0.6
0.4
0.2
0
0
5
10
15
20
Distance (mm)
15 Gy
1.5 Gy

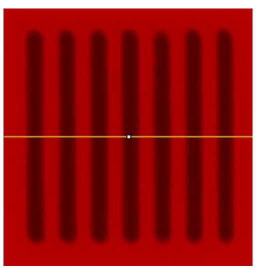

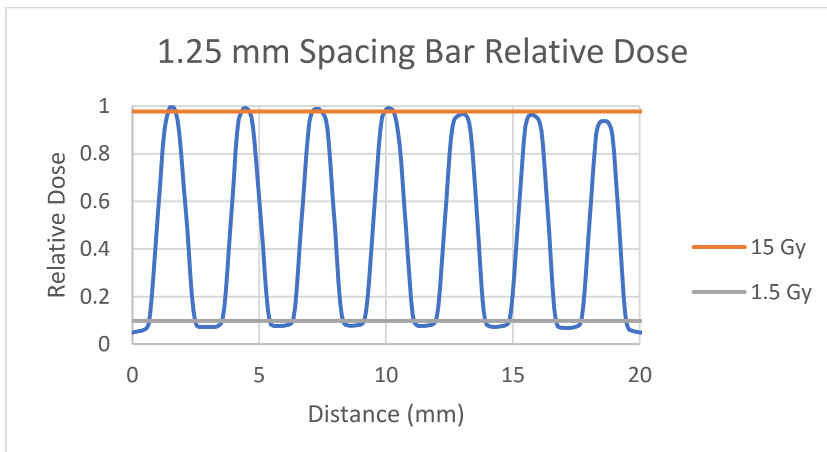
1.25 mm Spacing Bar Relative Dose
Relative Dose
1
0.8
0.6
0.4
0.2
0
0
5
10
15
20
Distance (mm)
15 Gy
1.5 Gy

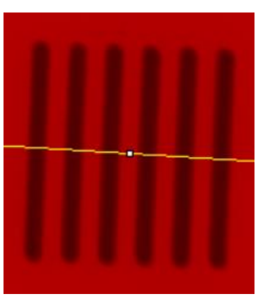

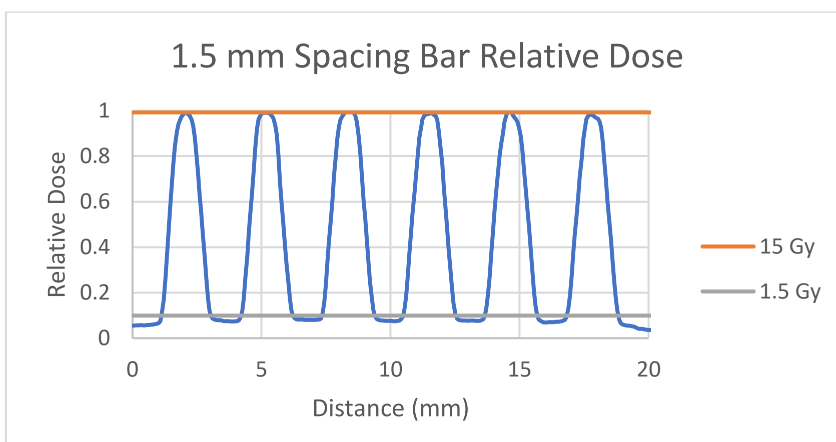
1.5 mm Spacing Bar Relative Dose
Relative Dose
1
0.8
0.6
0.4
0.2
0
0
5
10
15
20
Distance (mm)
15 Gy
1.5 Gy

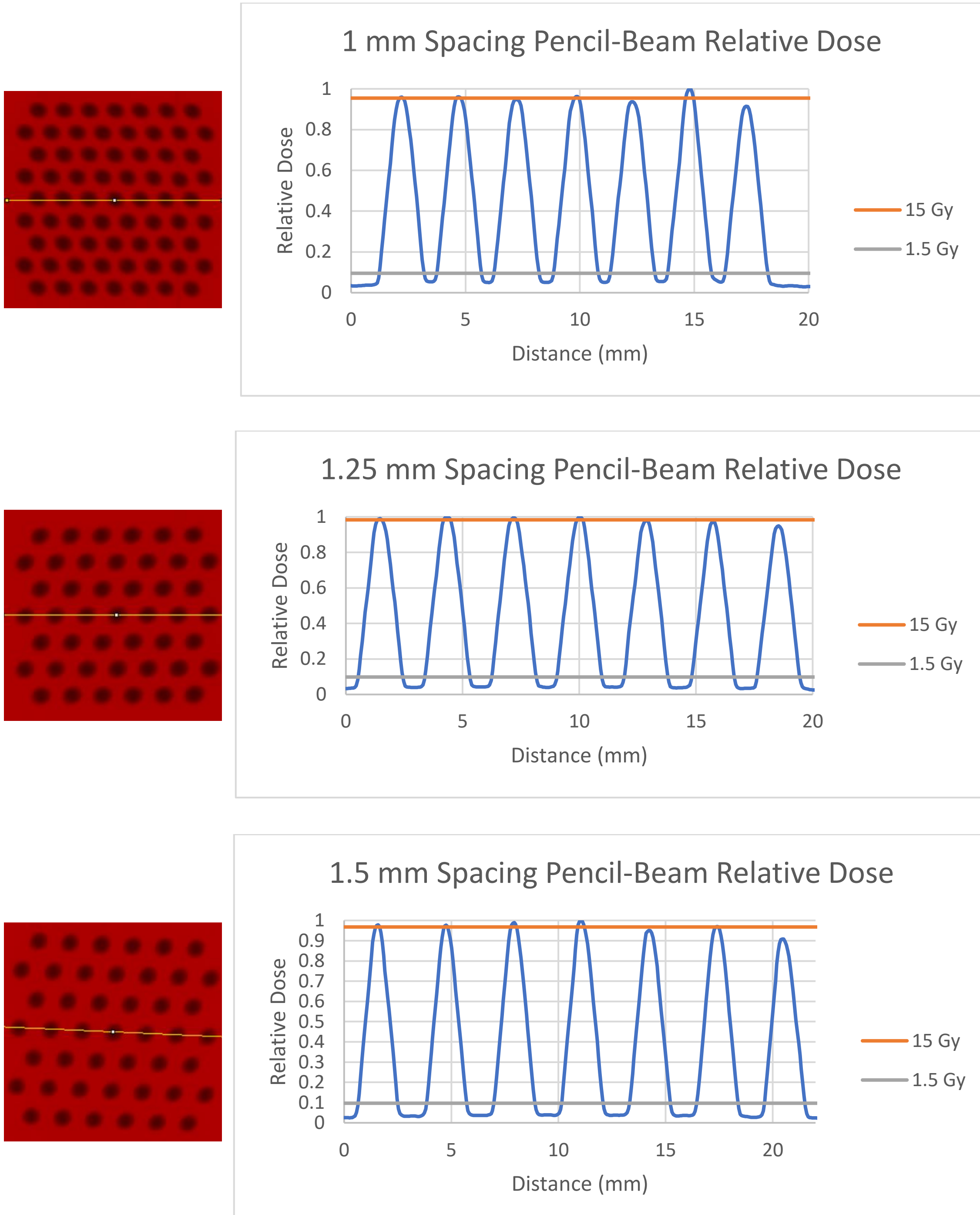

Figure 15: Line profiles through GRID dose distributions on Gafchromic film. Dose is normalized to the maximum dose along the profile. 15 Gy was the treatment dose in the preclinical trial and was prescribed to the average peak. 1.5 Gy is the dose to spare 50% of CD4+ and CD8+ T cells.

3.1.2 Quantitative analysis of dose distributions

3.1.2.1 Integral dose relative to open field

Integral dose quantifies the dose delivered to a treatment zone. Integral dose for each GRID relative to open fields of the same size are shown in Figure 15 and Table 2. All GRIDs deliver substantially less integral dose than an open field. The amount of integral dose delivered tends to be less than the open-to-closed ratio of each GRID. For example, the bar GRID with 1 mm beamlet spacing is 50% open (Table 1) but delivers and integral dose of 45.9% ± 0.4 compared to a completely open field (Table 2).

Table 2: Integral Dose.

GRID Pattern	Beamlet Spacing (mm)	Integral Dose Relative to Open Field
Bar	1	45.9% ± 0.4
	1.25	41.4% ± 0.4
	1.5	39.2% ± 0.1
Pencil Beam	1	23.9% ± 0.3
	1.25	17.9% ± 0.1
	1.5	16.3% ± 1.2

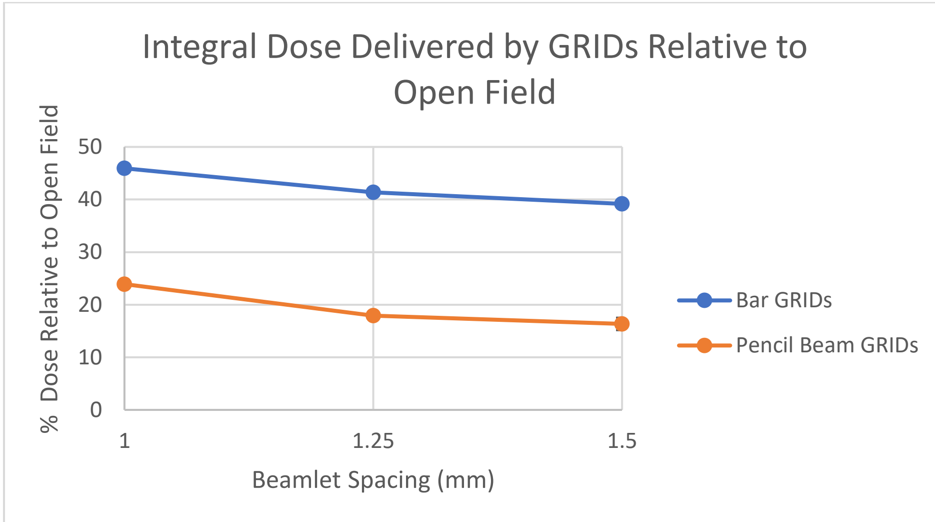

Figure 16: Integral dose delivered by each GRID relative to a same-sized open field.

3.1.2.2 Treatment area above and below dose thresholds

Results of dose map analysis are shown in Table 3 and Figure 17. Pencil-beam GRIDs produce low-dose regions that are almost twice are large as the low-dose regions in bar GRIDs with the same beamlet spacing. This trend suggests that pencil-beam patterns would spare many more intra-tumor lymphocytes, which could be advantageous for an immune response. However, bar GRIDs deliver high dose to a much greater amount of the tumor than pencil-beam GRIDs. When dose is prescribed to the average height of peaks, bar GRIDs deliver prescription dose to 3-5% of the tumor while pencil-beam GRIDs deliver prescription dose to less than 1% of the tumor. Therefore, these pencil-beam GRIDs may struggle to damage tumors with direct radiation damage. The volume receiving treatment dose would increase if beamlet spacing were decreased.

Table 3: Percent areas treated and spared by GRIDs. 1.5 Gy spares 50% of CD4+ and CD8+ T cells, and 3.1 Gy spares only 10%.

GRID Pattern	Beamlet Spacing (mm)	% Area Receiving <1.5 Gy	% Area Receiving <3.1 Gy	% Area Receiving ≥90% Dose	% Area Receiving ≥15 Gy
Bar	1	32.5 ± 0.6	41.8 ± 0.3	23.0 ± 0.6	4.2 ± 1.3
	1.25	41.3 ± 0.4	48.9 ± 0.3	20.9 ± 0.3	5.2 ± 0.4
	1.5	43.5 ± 0.1	51.0 ± 0.1	19.3 ± 0.1	2.5 ± 0.1
Pencil Beam	1	54.1 ± 0.2	64.4 ± 0.1	4.2 ± 0.2	0.4 ± 0.1
	1.25	67.4 ± 0.1	74.5 ± 0.1	3.1 ± 0.1	0.4 ± 0.1
	1.5	71.5 ± 0.9	78.0 ± 0.7	2.9 ± 0.4	0.8 ± 0.5

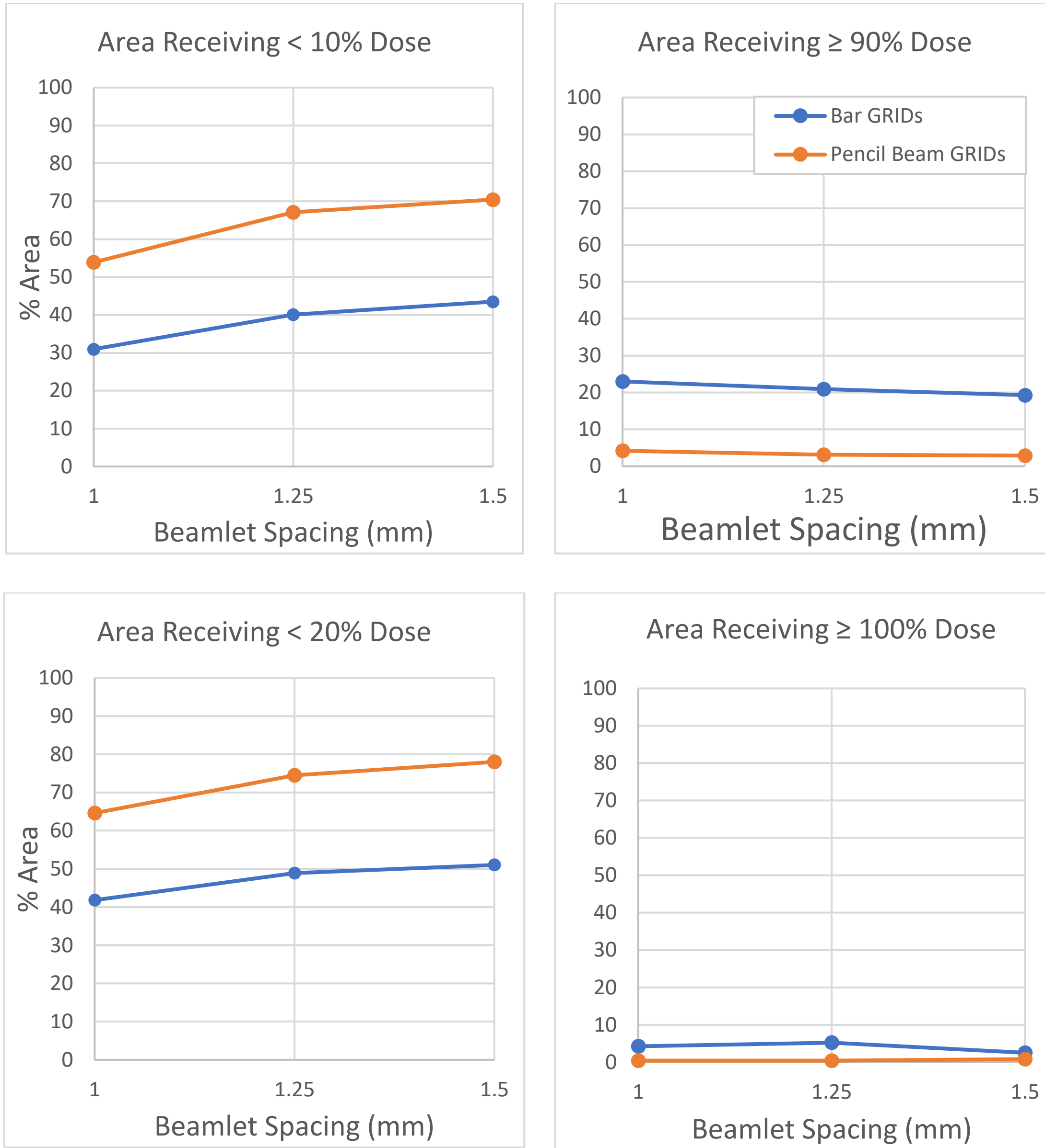

Figure 17: Tissue spared (left) and treated (right) by GRIDs.

3.1.2.3 Dose volume histogram results

DVHs for each GRID are shown in Figure 18. These curves are indicative of the dose distribution for approximately the first millimeter of tissue. Bar GRIDs deliver higher dose to the entire area for all dose levels. The pencil-beam designs have small areas receiving prescription dose, so their DVHs end at sharp points. Increasing spacing from 1 mm to 1.25 mm has a significant reduction of moderate doses, but the dose reduction from shrinking spacing further is less significant. This trend indicates that scatter reduction across beamlets has diminishing returns as spacing increases. These findings are consistent with the other observations.

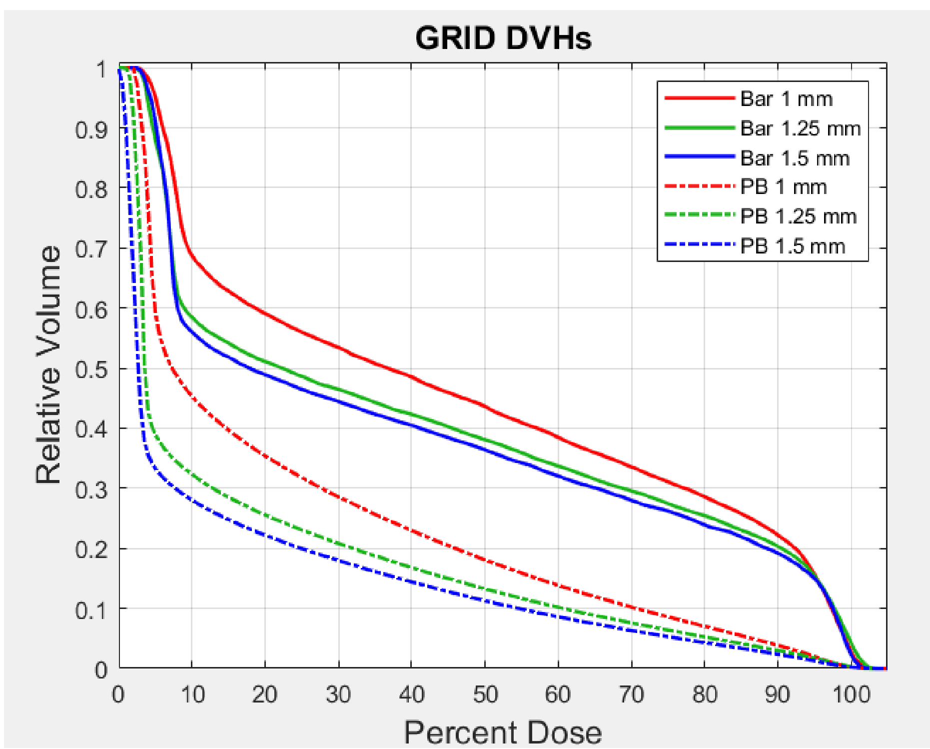

Figure 18: Dose volume histograms of GRIDs. "PB" stands for pencil beam. Lines are generated from dose maps.

3.1.2.4 An alternative method of prescribing dose

This trial prescribed dose to the average height of peaks in each GRID. As shown in Figure 17, the area receiving the prescription dose is very small: it is at most 5% for bar GRIDs and less than 1% for all pencil-beam GRIDs. To determine how many lymphocytes would be spared, we began with a dose prescription and found the dose reduction of the valleys. From a lymphocyte-sparing perspective, it would more straightforward to begin by prescribing a valley dose based on thresholds of lymphocyte sparing. For example, if a 50% lymphocyte sparing threshold were chosen, then 1.5 Gy would be prescribed to valleys and peaks dose would adjust accordingly. This method would allow for the optimization of peak doses and lymphocyte sparing for each GRID. Example doses delivered by this method are shown in Table 4, where 1.5 Gy and 3.1 Gy are prescribed to average valley height. These doses correspond to 50% and 10% lymphocyte sparing, respectively.

Table 4: Average peak doses given prescriptions to average valleys.

GRID Pattern	Beamlet Spacing (mm)	Avg. Peak Dose Given Valley Prescription (Gy)	
		1.5 Gy Valley Prescription (50% lymphocyte sparing)	3.1 Gy Valley Prescription (10% lymphocyte sparing)
Bar	1	17.9 ± 1.3	37.0 ± 2.8
	1.25	20.5 ± 0.6	42.3 ± 1.3
	1.5	20.6 ± 0.8	42.6 ± 1.6
Pencil Beam	1	28.0 ± 0.9	57.9 ± 1.8
	1.25	39.5 ± 2.3	81.5 ± 4.8
	1.5	46.5 ± 4.9	96.1 ± 10.2

3.1.3 Effects of depth on treatment setups

Two treatment setups were evaluated: the first is a standard setup where GRIDs are mounted in a block tray approximately 6 cm from isocenter, and in the second GRIDs are placed on top of a table 3 cm closer to the tumor. Figure 10 shows the evaluation of both setups.

An example of line profiles for each treatment setup are shown in Figure 19, which shows that the table setup created steeper dose gradients than the standard block tray setup.

Figure 20 displays the quantitative comparisons between the setups. Differences in peak-to-valley ratios were negligible, but the table setup halved the penumbral region and increased valley width by approximately 10%. These changes would increase sparing of lymphocytes, so the table setup was selected for preclinical trials.

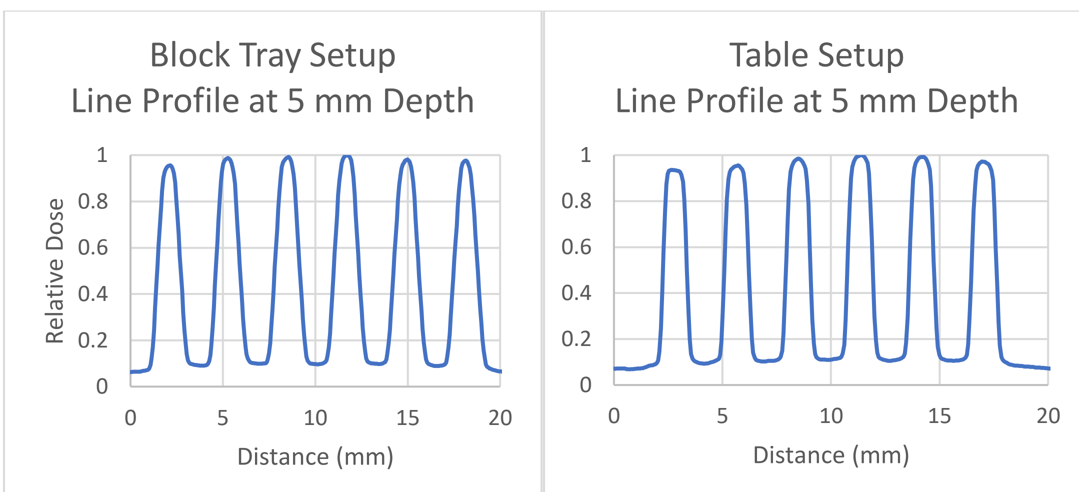

Figure 19: Example of dose distributions from a block tray and table setup for the same GRID. The bar GRID with 1.5 mm spacing was used.

a)
b)
c)

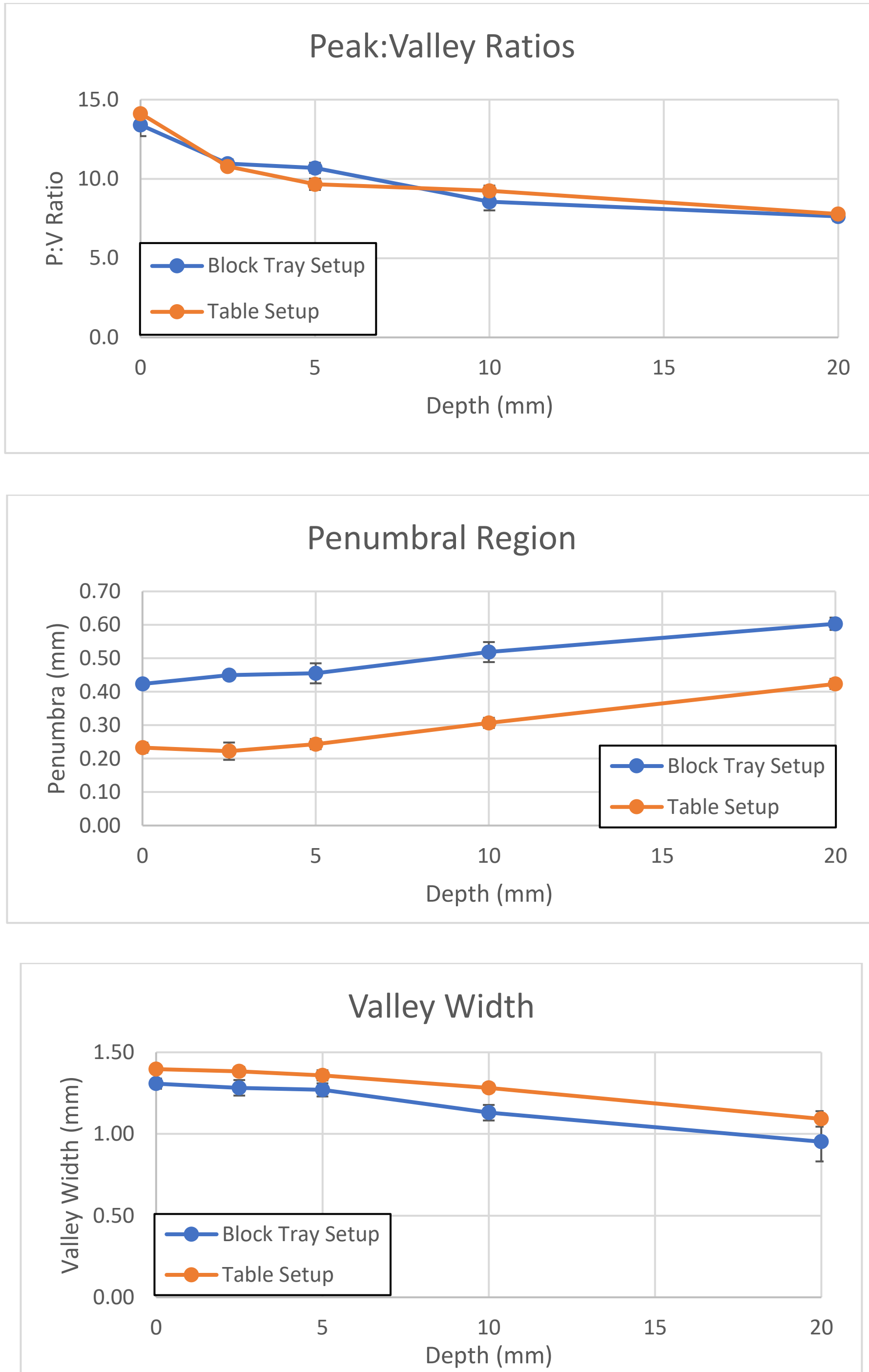

Figure 20: Effects of setup on dose distribution as depth increases. a) Peak:valley. b) Penumbral region (defined as 20-80% dose). c) Valley width (mm).

3.2 Quantitative evaluation of tumor motion effects on GRID Treatment

Table 5 documents the full width half maximums of beams in the motion trials. Beam widths found in the stationary trial were comparable to those on mouse tumors. Beam width was comparable between the stationary trial, the mouse with a tumor of standard treatment size, and both mice with no tumors. Average beam width was slightly larger in the trial using the mouse with a tumor of approximately 400 mm^3, which, is about four times larger than standard treatment size. The results suggest that motion may be a factor when tumors induced in the flank are extremely large. At worst, beams might broaden by 10% in a very large tumor compared to a stationary target. However, all mice in the preclinical trial had tumors of standard treatment size, so motion was considered negligible for the preclinical trial.

Table 5: Quantitative motion analysis. The standard tumor was approximately 70 mm^3 before irradiation, and the large tumor was approximately 400 mm^3 before irradiation.

	Stationary	Avg Motion	Standard Tumor	Large Tumor	No Tumor 1	No Tumor 2
FWHM (mm)	1.17 ± 0.05	1.19 ± 0.10	1.16 ± 0.05	1.24 ± 0.07	1.22 ± 0.03	1.16 ± 0.03

3.3 Preclinical Trial

3.3.1 Time to quintupling

Time to quintupling of tumor volume was chosen as the endpoint of this study. To date, nine tumors in the full irradiation group have not quintupled, but all other tumors have. Figure 21 shows a Kaplan-Meier estimate (AKA a survival curve) of all four treatment arms. Figure 22 shows a Kaplan-Meier estimate that excludes the AP control, which allows for convenient comparison of the other three groups. Table 6 contains the mean, median, minimum, and maximum time to quintupling for each group. The unirradiated control had the lowest values in every category. However, mean values had notable overlap in the unirradiated, hemi-irradiation, and GRID groups (means = 12 ± 2, 13 ± 4, and 14 ± 4 days, respectively).

Time to quintupling was statistically analyzed with log-rank tests between each group. This test calculates P values between each group. The P value represents that probability that the groups are the same, where a value of 1 is a 100% chance they are the same and zero is a 0% chance the groups are the same. The criteria for a significant difference between two groups is a P value less than 0.05. The full irradiation was very significantly different from the other groups ($P<0.001$). GRID and hemi-irradiation groups were not significantly different from each other ($P = 0.5257$). The GRID and hemi-irradiation groups also were not significantly different from the unirradiated group ($P = 0.122$ and $P = 0.2437$, respectively). The GRID's P-value indicates a 12.2% chance that the GRID and unirradiated groups are the same, which is higher than the significance threshold of 5%.

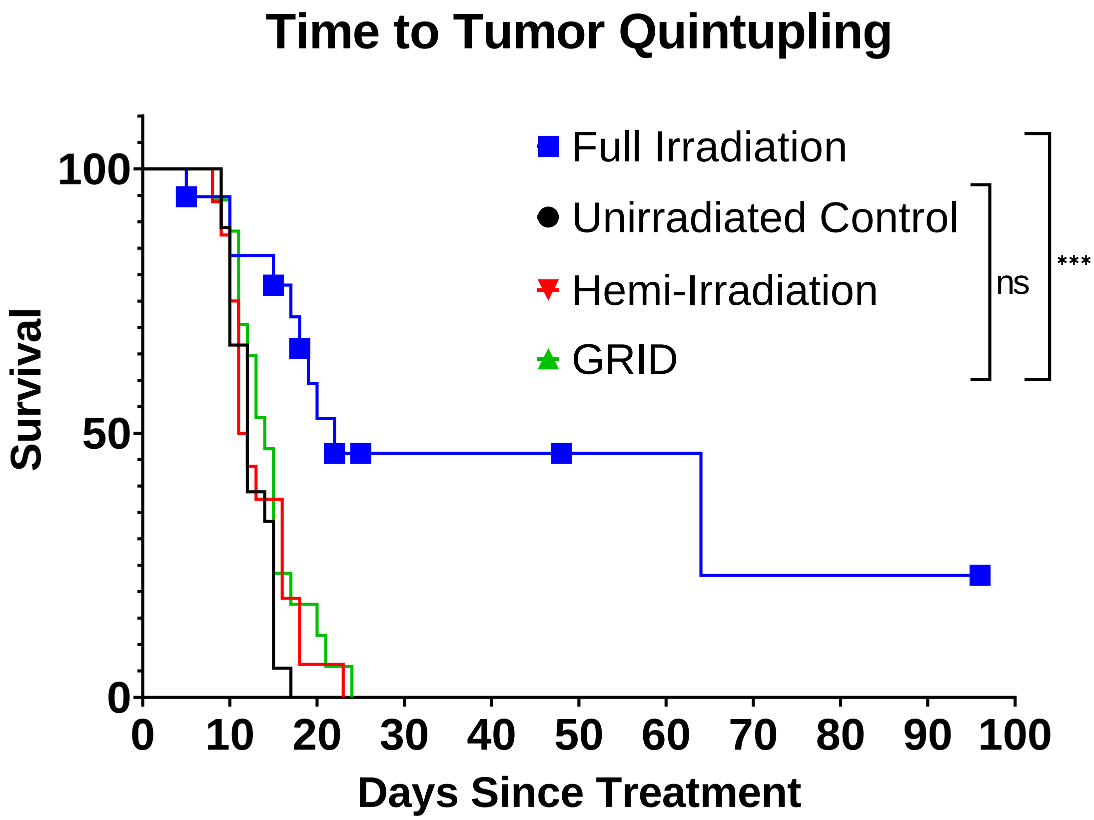

Figure 21: Kaplan-Meier chart of time to tumor quintupling. Nine mice full irradiation group have tumors that have not quintupled to date, and their most recent measurement days are indicated with markers.

Table 6: Quantitative time to tumor quintupling metrics. All values are in days.

Metric	Unirradiated	Full Irrad.	Hemi-Irrad.	GRID
Mean	12 ± 2	20 ± 16	13 ± 4	14 ± 4
Median	12	18	12	14
Min	9	5	8	8
Max	17	64	23	24

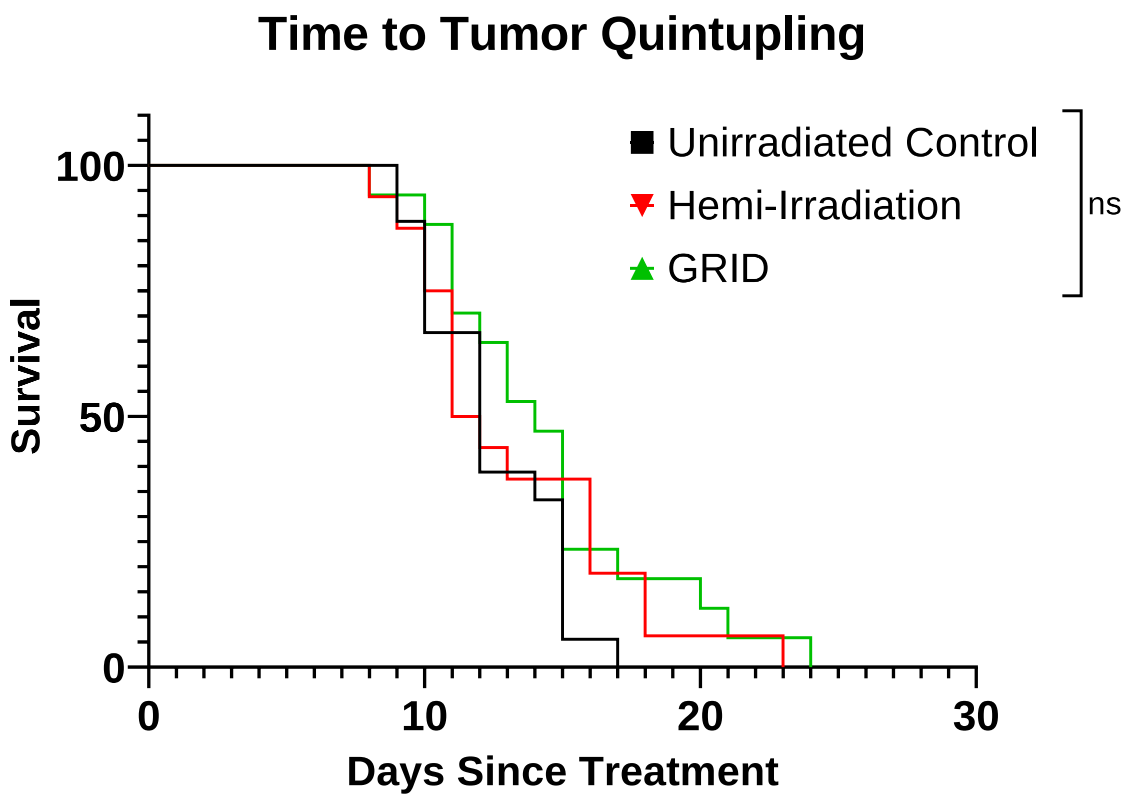

Figure 22: Kaplan-Meier chart without the full irradiation group.

3.3.2 Tumor growth curves

Figure 23 displays the tumor growth of all the mice in the four treatment groups. For convenience, Figure 24 shows each treatment group on a separate curve. These curves indicate a high variance in GRID and hemi-irradiation groups.

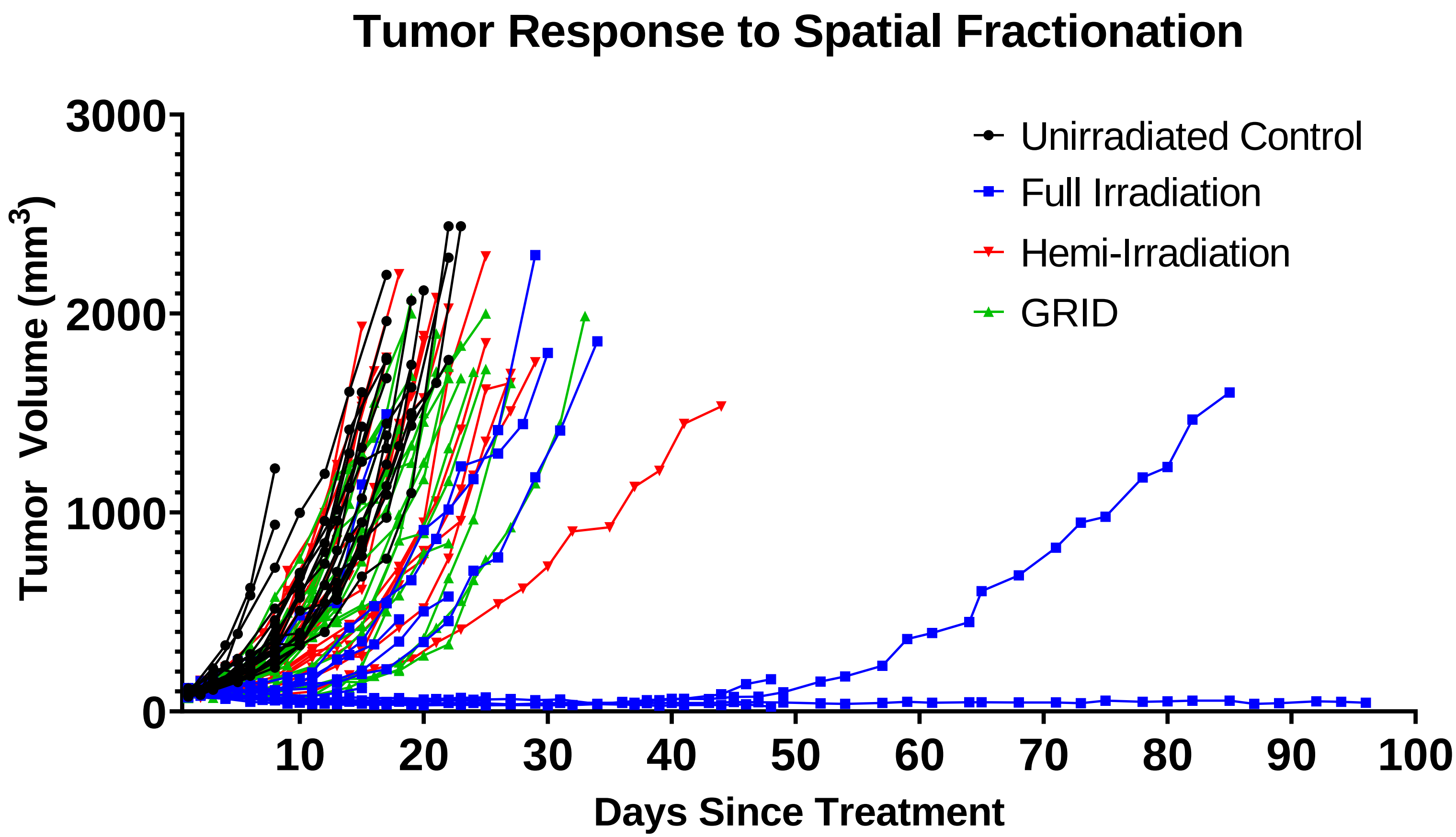

Figure 23: Tumor volume after treatment for all mice.

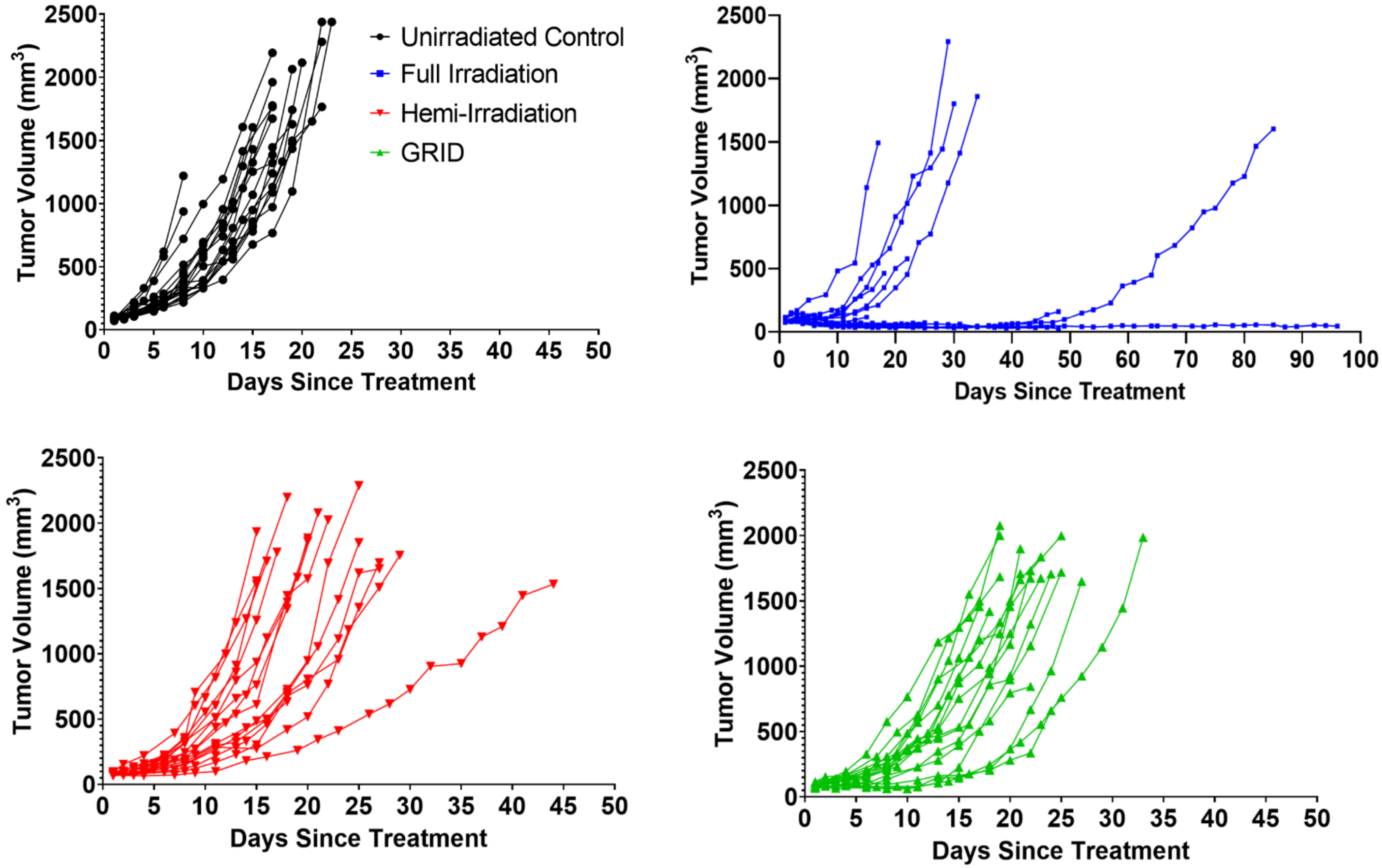

Figure 24: Independent graphs of tumor growth. Note that the AP group extends to 100 days.

3.3.3 Initial tumor volume

To eliminate biases in the selection of mice for each group, the initial tumor volume of each mouse was documented. Figure 25 shows box and whisker plots for each group. The hemi-irradiation group has a higher concentration of small-volume tumors, but all are within the size limits of standard treatments.

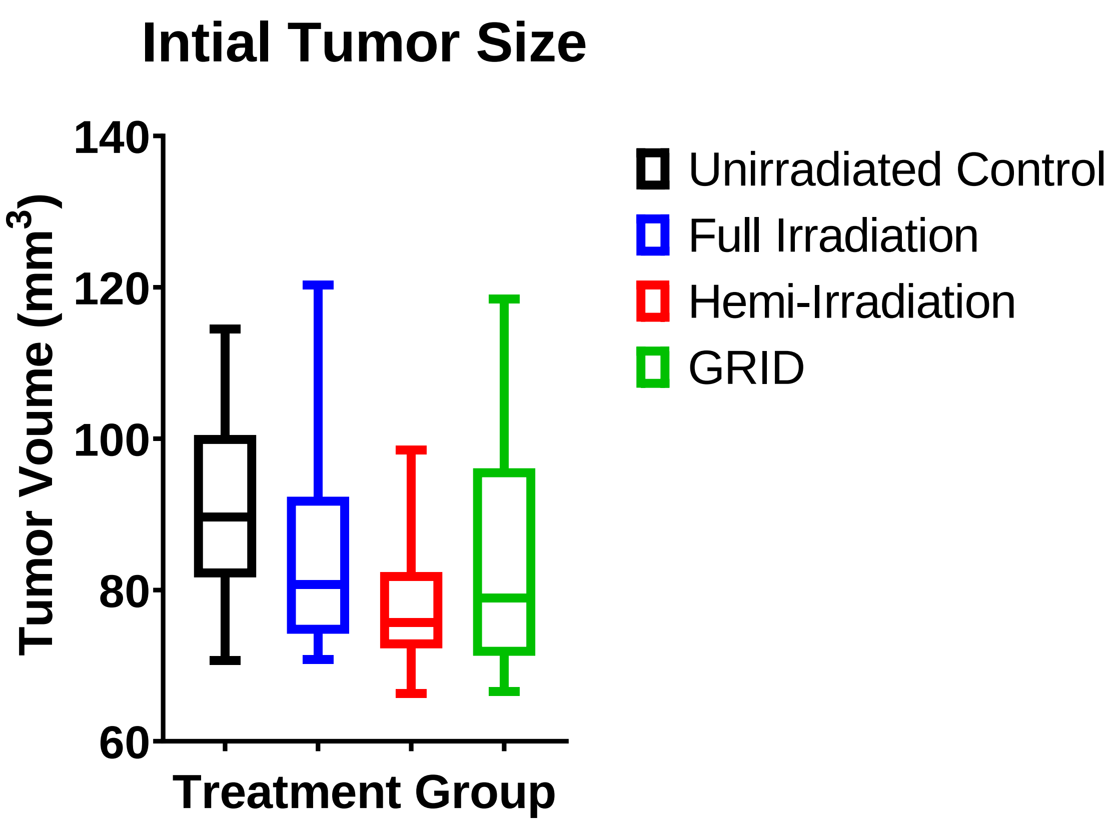

Figure 25: Distributions of initial tumor volumes for each treatment group. The horizontal bar within each box indicates the mean volume of that group.

4. Conclusions

4.1 GRID design

4.1.1 Bars vs pencil beams

This study compares the dosimetric qualities of bar and pencil-beam GRIDs. Prescription dose level was defined as the average peak height of each GRID. Pencil-beam GRIDs had very high peak to valley ratios and delivered less than 10% peak dose to 50-70% of the tumor. For a 15 Gy prescription to average peak height, those GRIDs could spare 25-35% of CD4+ and CD8+ T cells in the treatment zone. However, pencil beams would deliver prescribed dose to less than 1% of the tumor. In contrast, bar GRIDs had lower peak-to-valley ratios and delivered less than 10% peak dose to 30-40% of the treatment area, but they delivered prescription dose to 3-5% of the tumor.

Due to steep dose gradients, the amount of tissue receiving at least 95% prescription dose is significantly higher than the amount of tissue receiving 100% of the prescription or more. The area above 95% dose was 2-2.5% for pencil-beam GRIDs and 15-20% for bar GRIDs.

The above descriptions use average peak height as the point of prescription. However, and alternative method (outlined in section 3.1.2.3) would be to prescribe a lymphocyte-sparing dose the average valley height. If a treatment goal was to preserve 50% of lymphocytes, 1.5 Gy would be prescribed to the valley. Bar GRIDs would have peak doses of 18-21 Gy, and pencil-beam GRIDs would have peak doses of approximately 28, 40, and 47 Gy for 1, 1.25, and 1.5 mm beamlet spacing. For a 3.1 Gy valley dose, which would spare 10% of lymphocytes, peak dose would increase substantially to 37-43 Gy for bar GRIDs and 57.9 ± 1.8, 81.5 ± 4.8, 96.1 ± 10.2 Gy for pencil-beam GRIDs with spacings of 1, 1.25, and 1.5 mm, respectively.

4.1.2 Comparison to GRIDs in other studies

The kV GRIDs created in this experiment create significantly higher peak-to-valley ratios than MV GRIDs in historical trials. The first dosimetrically analyzed MV GRID had a peak-to-valley ratio of 2.5 (Reiff et al. 1995), and a GRID in 2010 trials had a peak-to-valley ratio of 6.3 (Buckey et al. 2010). Those MV GRIDs treated 50% of the tumors, and our bar GRID with 1 mm beamlet spacing treated the same proportion of the target with a peak-to-valley ratio of 11.9 ± 0.9.

In a 2017 study, the only other kV GRID used in preclinical trials was developed and analyzed (Bazyar et al. 2017). It was a bar pattern that treated 33% of the target, and it achieved a peak-to-valley ratio of 24.35 ± 2.10. The GRID in that trial had a higher peak-to-valley ratio than either of our GRIDs with similar proportions of treated area. It was able to achieve such a high ratio because it was made of 5 mm thick lead ribbons whereas ours GRIDs were machined from 3 mm thick lead sheets.

4.1.3 Evaluation of treatment setups

The dosimetry comparison between a block tray setup and a table setup found advantages to placing the GRID close to the tumor. The proximal placement reduced beam divergence after collimation by the GRID, which halved the penumbral region of the beams and increased valley widths by 10%. Therefore, placing GRIDs close to the tumor may increase lymphocyte and normal tissue sparing.

4.2 Motion in GRID trials

Motion was deemed negligible when tumors were induced in the flank and were of standard treatment size. When a mouse with a very large tumor (~4 times standard treatment size) was treated, mean beam width increased by 6%. This result suggests that motion could be a factor if extremely large tumors were treated, which could blur the dose distribution, reduce peak dose, and increase valley dose. If future trials are performed on tumors in other locations, motion should be evaluated before GRID treatments.

4.3 Preclinical trial of spatial fractionation

GRID therapy and hemi-irradiation had insignificant delays in time to tumor quintupling compared to unirradiated mice ($P = 0.122$ and $P = 0.2437$, respectively). GRID therapy was not a substitution for conventional RT in this mouse model for the same dose level. The GRID treatment technique used in this study may require a significant overhaul to be comparable to a conventional treatment.

The hemi-irradiation of C57BL/6 mice with p53/MCA transplant sarcoma does not replicate the findings of Markovsky et al. 2019, which found that hemi-irradiation results were indifferentiable from conventional RT in 67NR breast cancer in BALB/C mice and Lewis lung cancer in C57BL/6 mice. The Markovsky study had treatment arms of 10, 15, and 20 Gy, so our 15 Gy hemi-irradiation should be comparable. It is possible that the immune response documented in the Markovsky study is tumor-dependent, and our sarcoma model does not have the same microenvironment.

4.4 Future investigations

A 15 Gy treatment using the bar GRID with 1 mm beamlet spacing was not as effective at controlling tumors as a 15 Gy conventional treatment. A direct replacement of conventional RT with GRID therapy at the same dose level has not been attempted in other studies. In human patients, GRID has only been used as a single-fraction boost to conventional RT treatments (multiple studies summarized in Yan et al. 2019). GRID as a boost has not been attempted in mice trials.

A core benefit of GRID therapy and other spatial fractionation techniques is reduction in normal tissue complications (Griffin et al. 2020). Human patients in GRID trials have shown no skin minimal skin effects despite single-shot doses of 10-25 Gy. A bar GRID study in mice used a 4x10 cm array of 0.3 mm beamlets with 0.6 mm spacing, and it delivered 150 Gy with no apparent complications (Bazyar et al. 2017). A study of a single 1 mm kV beam delivering 60 Gy found no indications of redness, swelling, or other complications in mouse ears (Sammer et al. 2019). Our trial did not evaluate normal tissue effects in any treatment arm, but our GRIDs adhered to the Sammer study by using 1 mm beams. Increasing the dose of GRID treatments above the dose of conventional RT may improve tumor control outcomes without damaging healthy tissue. An example treatment might prescribe 1.5 Gy to valleys for lymphocyte sparing, which would increase peak dose to 18-21 Gy for bar GRIDs or 30-50 Gy for pencil-beam GRIDs, depending on the selected beamlet spacing. These high doses would still be below the 60 Gy of the Sammer study, although a single pencil beam was used instead of an array of beams. Of any potential future investigation, GRID therapy with a higher dose has the most pre-existing evidence.

Several completely unexplored aspects of GRID therapy remain. All GRID human and mouse trials to date have used single, high-dose fractions. GRID therapy may be able to administer several fractions of high dose. Additionally, the direct impact of GRID therapy on lymphocytes has not been evaluated. If GRID achieves positive treatment outcomes in a future trial, it may be valuable to perform flow cell cytometry or immunohistochemistry to quantify the number of intra-tumor lymphocytes relative to control groups. Lastly, if GRID therapy can be an immunostimulatory treatment technique, it may be paired with immunotherapy techniques such as checkpoint blockade therapy.

References

Asur, Rajalakshmi S., Sunil Sharma, Ching-Wei Chang, Jose Penagaricano, Indira M. Kommuru, Eduardo G. Moros, Peter M. Corry, and Robert J. Griffin. “Spatially Fractionated Radiation Induces Cytotoxicity and Changes in Gene Expression in Bystander and Radiation Adjacent Murine Carcinoma Cells.” Radiation Research 177, no. 6 (June 2012): 751–65. https://doi.org/10.1667/rr2780.1.

Bazyar, Soha, Christina R Inscoe, E Timothy O’Brian, Otto Zhou, and Yueh Z Lee. “Minibeam Radiotherapy with Small Animal Irradiators; *in Vitro* and *in Vivo* Feasibility Studies.” *Physics in Medicine & Biology* 62, no. 23 (November 10, 2017): 8924–42. https://doi.org/10.1088/1361-6560/aa926b.

Bouchet, Audrey, Nathalie Sakakini, Michèle El Atifi, Céline Le Clec’h, Elke Brauer, Anaïck Moisan, Pierre Deman, Pascal Rihet, Géraldine Le Duc, and Laurent Pelletier. “Early Gene Expression Analysis in 9L Orthotopic Tumor-Bearing Rats Identifies Immune Modulation in Molecular Response to Synchrotron Microbeam Radiation Therapy.” *PLOS ONE* 8, no. 12 (December 31, 2013): e81874. https://doi.org/10.1371/journal.pone.0081874.

Bouchet, Audrey, Raphäel Serduc, Jean Albert Laissue, and Valentin Djonov. “Effects of Microbeam Radiation Therapy on Normal and Tumoral Blood Vessels.” *Physica Medica*, Radiation Therapy with Synchrotron Radiation: Achievements and Challenges, 31, no. 6 (September 1, 2015): 634–41. https://doi.org/10.1016/j.ejmp.2015.04.014.

Buckey, Courtney, Sotirios Stathakis, Ken Cashon, Alonso Gutierrez, Carlos Esquivel, Chengyu Shi, and Nikos Papanikolaou. “Evaluation of a Commercially-Available Block for Spatially Fractionated Radiation Therapy.” *Journal of Applied Clinical Medical Physics* 11, no. 3 (June 2010): 2–11. https://doi.org/10.1120/jacmp.v11i3.3163.

Chakraborty, Mala, Scott I. Abrams, C. Norman Coleman, Kevin Camphausen, Jeffrey Schlom, and James W. Hodge. “External Beam Radiation of Tumors Alters Phenotype of Tumor Cells to Render Them Susceptible to Vaccine-Mediated T-Cell Killing.” Cancer Research 64, no. 12 (June 15, 2004): 4328–37. https://doi.org/10.1158/0008-5472.CAN-04-0073.

Demaria, Sandra, Bruce Ng, Mary Louise Devitt, James S Babb, Noriko Kawashima, Leonard Liebes, and Silvia C Formenti. “Ionizing Radiation Inhibition of Distant Untreated Tumors (Abscopal Effect) Is Immune Mediated.” *International Journal* *of Radiation Oncology*Biology*Physics* 58, no. 3 (March 1, 2004): 862–70. https://doi.org/10.1016/j.ijrobp.2003.09.012.

Edwards, J. M., P. H. Shah, J. L. Huhn, W. St. Clair, W. F. Regine, M. Mohiuddin, and M. R. Kudrimoti. "Definitive GRID and Fractionated Radiation in Bulky Head and Neck Cancer Associated With Low Rates of Distant Metastasis." *International Journal of Radiation Oncology*Biology*Physics*, Proceedings of the American Society for Radiation Oncology 57th Annual Meeting, 93, no. 3, Supplement (November 1, 2015): E334. https://doi.org/10.1016/j.ijrobp.2015.07.1399.

Griffin, Robert J., Mansoor M. Ahmed, Beatriz Amendola, Oleg Belyakov, Søren M. Bentzen, Karl T. Butterworth, Sha Chang, et al. "Understanding High-Dose, Ultra-High Dose-Rate and , Spatially Fractionated Radiotherapy." *International Journal of Radiation Oncology*Biology*Physics*, April 13, 2020. https://doi.org/10.1016/j.ijrobp.2020.03.028.

Hu, Qian, Yujie Xie, Yuanlong Ge, Xin Nie, Jun Tao, and Yong Zhao. "Resting T Cells Are Hypersensitive to DNA Damage Due to Defective DNA Repair Pathway." Cell Death & Disease 9, no. 6 (May 31, 2018): 662. https://doi.org/10.1038/s41419-018-0649-z.

Kanagavelu, S., S. Gupta, X. Wu, S. Philip, M.M. Wattenberg, J.W. Hodge, M.D. Couto, K.D. Chung, and M.M. Ahmed. "In Vivo Effects of Lattice Radiation Therapy on Local and Distant Lung Cancer: Potential Role of Immunomodulation." *Radiation Research* 182, no. 2 (2014): 149–62. https://doi.org/10.1667/RR3819.1.

Kaur, Punit, and Alexzander Asea. "Radiation-Induced Effects and the Immune System in Cancer." Frontiers in Oncology 2 (2012). https://doi.org/10.3389/fonc.2012.00191.

Markovsky, Ela, Sadna Budhu, Robert M. Samstein, Hongyan Li, James Russell, Zhigang Zhang, Esther Drill, et al. "An Antitumor Immune Response Is Evoked by Partial-Volume Single-Dose Radiation in 2 Murine Models." *International Journal of Radiation Oncology*Biology*Physics* 103, no. 3 (March 1, 2019): 697–708. https://doi.org/10.1016/j.ijrobp.2018.10.009.

Mohiuddin, M., D.L. Curtis, W.T. Grizos, and L. Komarnicky. "Palliative Treatment of Advanced Cancer Using Multiple Nonconfluent Pencil Beam Radiation: A Pilot Study." *Cancer* 66, no. 1 (1990): 114–18. https://doi.org/10.1002/1097-0142(19900701)66:1<114::AID-CNCR2820660121>3.0.CO;2-L.

Mohiuddin, Mohammed, James H. Stevens, Jay E. Reiff, M. Saiful Huq, and Nagalingam Suntharalingam. "Spatially Fractionated (GRID) Radiation for Palliative Treatment of Advanced Cancer." *Radiation Oncology Investigations* 4, no. 1 (1996): 41–47. https://doi.org/10.1002/(SICI)1520-6823(1996)4:1<41::AID-ROI7>3.0.CO;2-M.

Mohiuddin, Mohammed, Mihoko Fujita, William F Regine, Ali S Megooni, Goeffrey S Ibbott, and Mansoor M Ahmed. "High-Dose Spatially-Fractionated Radiation (GRID): A New Paradigm in the Management of Advanced Cancers." *International Journal of Radiation Oncology*Biology*Physics* 45, no. 3 (October 1, 1999): 721–27. https://doi.org/10.1016/S0360-3016(99)00170-4.

Nakamura, Nori, Yoichiro Kusunoki, and Mitoshi Akiyama. "Radiosensitivity of CD4 or CD8 Positive Human T-Lymphocytes by an in Vitro Colony Formation Assay." *Radiation Research* 123, no. 2 (1990): 224–27. https://doi.org/10.2307/3577549.

Neuner, Geoffrey, Majid M. Mohiuddin, Noam Vander Walde, Olga Goloubeva, Jonathan Ha, Cedric X. Yu, and William F. Regine. "High-Dose Spatially Fractionated GRID Radiation Therapy (SFGRT): A Comparison of Treatment Outcomes With Cerrobend vs. MLC SFGRT." *International Journal of Radiation Oncology*Biology*Physics* 82, no. 5 (April 1, 2012): 1642–49. https://doi.org/10.1016/j.ijrobp.2011.01.065.

Newton, Joseph, Mark Oldham, Andrew Thomas, Yifan Li, John Adamovics, David G. Kirsch, and Shiva Das. "Commissioning a Small-Field Biological Irradiator Using Point, 2D, and 3D Dosimetry Techniques." Medical Physics 38, no. 12 (December 2011): 6754–62. https://doi.org/10.1118/1.3663675.

Reiff, Jay E., M. Saiful Huq, Mohammed Mohiuddin, and Nagalingam Suntharalingam. "Dosimetric Properties of Megavoltage Grid Therapy." *International Journal of Radiation Oncology*Biology*Physics* 33, no. 4 (November 1, 1995): 937–42. https://doi.org/10.1016/0360-3016(95)00114-3.

Sammer, Matthias, Katharina Teiluf, Stefanie Girst, Christoph Greubel, Judith Reindl, Katarina Ilicic, Dietrich W. M. Walsh, et al. "Beam Size Limit for Pencil Minibeam Radiotherapy Determined from Side Effects in an In-Vivo Mouse Ear Model." *PLoS ONE* 14, no. 9 (September 4, 2019). https://doi.org/10.1371/journal.pone.0221454.

Serduc, Raphaël, Audrey Bouchet, Elke Bräuer-Krisch, Jean A. Laissue, Jenny Spiga, Sukhéna Sarun, Alberto Bravin, et al. "Synchrotron Microbeam Radiation

Therapy for Rat Brain Tumor Palliation—Influence of the Microbeam Width at Constant Valley Dose." *Physics in Medicine & Biology* 54, no. 21 (October 20, 2009): 6711. https://doi.org/10.1088/0031-9155/54/21/017.

Ślosarek, Krzysztof, Wojciech Osewski, Aleksandra Grządziel, Michał Radwan, Łukasz Dolla, Marta Szlag, and Małgorzata Stąpór-Fudzińska. "Integral Dose: Comparison between Four Techniques for Prostate Radiotherapy." Reports of Practical Oncology and Radiotherapy: Journal of Greatpoland Cancer Center in Poznan and Polish Society of Radiation Oncology 20, no. 2 (April 2015): 99–103. https://doi.org/10.1016/j.rpor.2014.10.010.

Sologuren, Ithaisa, Carlos Rodríguez-Gallego, and Pedro Carlos Lara. "Immune Effects of High Dose Radiation Treatment: Implications of Ionizing Radiation on the Development of Bystander and Abscopal Effects." *Translational Cancer Research* 3, no. 1 (February 25, 2014): 18-31–31. https://doi.org/10.21037/2091.

Treibel, Franziska, Mai Nguyen, Mabroor Ahmed, Annique Dombrowsky, Jan J. Wilkens, Stephanie E. Combs, Thomas E. Schmid, and Stefan Bartzsch. "Establishment of Microbeam Radiation Therapy at a Small Animal Irradiator." *International Journal of Radiation Oncology, Biology, Physics* 0, no. 0 (October 6, 2020). https://doi.org/10.1016/j.ijrobp.2020.09.039.

Tubin, Slavisa, Helmut H. Popper, and Luka Brcic. "Novel Stereotactic Body Radiation Therapy (SBRT)-Based Partial Tumor Irradiation Targeting Hypoxic Segment of Bulky Tumors (SBRT-PATHY): Improvement of the Radiotherapy Outcome by Exploiting the Bystander and Abscopal Effects." *Radiation Oncology* 14, no. 1 (January 29, 2019): 21. https://doi.org/10.1186/s13014-019-1227-y.

Yan, Weisi, Mohammad K. Khan, Xiaodong Wu, Charles B. Simone, Jiajin Fan, Eric Gressen, Xin Zhang, et al. "Spatially Fractionated Radiation Therapy: History, Present and the Future." *Clinical and Translational Radiation Oncology* 20 (October 22, 2019): 30–38. https://doi.org/10.1016/j.ctro.2019.10.004.